Chemical mass transfer in magmatic processes

II. Applications in equilibrium crystallization, fractionation and assimilation

Mark S. Ghiorso[1] and Ian S.E. Carmichael[2]

[1] Department of Geological Sciences, University of Washington, Seattle, WA 98195, USA
[2] Department of Geology and Geophysics, University of California, Berkeley, CA 94720, USA

Abstract. Numerical examples of the approach described in Part I of this series (Ghiorso, 1985) are presented in this paper. These examples include the calculation of the compositions and proportions of liquid and solid phases produced during (1) the equilibrium crystallization of a basaltic andesite at 1 bar, (2) the fractional crystallization of an olivine tholeiite at 1 bar and elevated pressures, (3) the fractional and equilibrium crystallization of an olivine boninite at 1 bar, and (4) the (a) isothermal and (b) isenthalpic assimilation of olivine (Fo_{90}) into a liquid/solid assemblage of quartz dioritic composition at $\sim 1{,}125°$ C and 3 kbars. The numerical results on the crystallization of the basaltic andesite are verified by comparison with experimental data while those calculations performed using olivine tholeiitic and olivine boninitic compositions are favorably compared against whole rock and mineral analytical data and petrographic and field observations.

In each of the examples presented, the heat effects associated with the modelled process are calculated (e.g. heat of crystallization, heat of assimilation), and free energies of crystallization are examined as a function of the degree of mineral supersaturation. The former quantities are on the order of 173 cal/grm for the cooling and fractional crystallization of an olivine tholeiite to a rhyolitic residuum (corresponding to a 400° C temperature interval). The latter represents an important petrological parameter, in that it quantifies the driving force for the rate of crystal growth and rate of nucleation in magmatic systems. Calculated free energies of crystallization are small (on the order of hundreds of calories per mole per 25° C of undercooling) which indicates that the kinetics of crystallization in magmatic systems are affinity controlled.

Melt oxygen fugacity and the degree of oxygen metasomatism play a major role in controlling the fractionation trends produced from crystallizing basaltic liquids. Calculations suggest that in order to generate a silica rich residuum *and* the characteristic iron enrichment trend during the fractional crystallization of a tholeiitic basalt, the magma must crystallize esentially along an f_{O_2} buffer. This buffered state can be maintained by exchange of oxygen (via hydrogen diffusion) between the magma and the surrounding country rocks or by magmatic oxidation-reduction equilibria. Additional calculations indicate the possibility that oxygen exchange may be unnecessary if the magma contains sufficient sulfur to maintain the system along an S_2/SO_2 oxygen buffer during the initial stages of crystallization.

Offprint requests to: M.S. Ghiorso

Introduction

In the first paper of this series (Ghiorso 1985, hereafter Part I) a computational algorithm is outlined for the modelling of equilibrium crystallization, crystal fractionation and solid phase assimilation in magmatic systems. This algorithm incorporates thermodynamic models for the solid and liquid phase solution properties (Ghiorso et al. 1983) and utilizes Gibbs and Korzhinskii potential function minimization techniques to describe stable multi-phase equilibria in both closed an open magmatic systems. Numerical results, obtained from applying this algorithm to a wide variety of petrological problems, are presented in this paper and are compared to natural rock data and experimental phase equilibria. These calculations represent the first attempt to model chemical mass transfer thermodynamically in crystallizing silicate solutions that have compositions which are essentially equivalent to magmas.

The purpose of this paper is twofold. The first is to demonstrate the computational effectiveness and the petrological applicability of the Part I algorithm. To this end, crystallization calculations are performed on three different varieties of basalt: (1) a basaltic andesite from Jorullo, Mexico, (2) an olivine tholeiite from Iceland, and (3) an "olivine boninite" from a marginal sill adjacent to the Bushveld Intrusion of South Africa. The second purpose of this paper is to emphasize the advantages of a thermodynamic description of phase equilibria in an evolving magmatic system. These advantages center around the ancillary information available during the course of crystallization concerning system state functions such as volume, enthalpy and heat capacity. Density differences between solid and liquid phases can be examined as a function of crystallization history as can other thermodynamic quantities such as the latent heat of crystallization. As an example of a petrological problem that can be solved only through thermodynamic analysis, we will present a detailed calculation of the volume changes and heat effects produced during the assimilation of olivine into a liquid of quartz dioritic composition.

All of the calculations reported in this paper were performed using the computer program SILMIN which is available from the first author[1]. The phase equilibria con-

sidered by this program are discussed in the Appendix to Part I.

In the discussion that follows, it will be important to keep two general aspects of these calculations in mind. The first is that the calculated stabilization energy of a solid-liquid magmatic phase assemblage in heterogeneous equilibrium is generally less than 5.0 cals/g more negative than a homogeneous metastable liquid of equivalent bulk composition, at the corresponding temperature and pressure. This small energy difference persists in melts which are up to 50% crystallized (see below)! The geochemical implication is that the chemical affinity that drives crystallization processes in igneous systems is small and of the order of (1) the free energy of mixing of most mineral solid solutions, or (2) the activation energies for transport, nucleation or crystal growth. This observation is in complete contrast to mineral-fluid interactions commonly observed in aqueous systems and emphasizes the importance of crystallization kinetics in magmatic systems and the role the chemical affinity must play in describing the rate laws for these processes.

The second important aspect of the calculations to be presented concerns the oxidation state of iron in the melt. It is widely recognized (e.g. Osborn 1959, 1962) that profoundly different crystallization sequences can arise from liquid compositions with widely varying ferric/ferrous ratios but otherwise identical bulk compositions. However, it is not generally appreciated that a related, but somewhat more subtle effect, occurs in the fractional crystallization of a closed magmatic system, where the act of crystallizing iron-bearing phases can have a major influence upon the melt ferric/ferrous ratio and hence the sequence of crystallization. The calculations presented below demonstrate these

phenomena and place severe restrictions on the applicability of closed or open (to oxygen) system modelling of magmatic processes. The petrologic question of a locally restricted or generally pervasive oxygen fugacity will be a reoccurring theme in the discussion that follows.

The first part of this paper will consider examples of the calculation of the equilibrium and fractional crystallization of basaltic lavas. The final section will treat the more complicated, and somewhat more controversial, results concerning the magmatic assimilation of solid phases.

Examples of equilibrium crystallization/crystal fractionation calculations at 1 bar and elevated pressures

Equilibrium crystallization of a basaltic andesite

Our first example is designed to demonstrate aspects of modelling equilibrium crystallization. For this purpose we have chosen to simulate numerically some recent experimental work on the 1 bar equilibrium crystallization of a basaltic andesite from Jorullo Volcano, Mexico (Table 1; Jor 44, Mo and Carmichael 1985). The simulation of these experimental results will also serve to indicate the advantages and the disadvantages of the computational scheme proposed in Part I. In this respect it is important to verify the utility of the Part I algorithm before attempting to calculate natural crystallization sequences, where magmatic intensive variables and the compositions of coexisting phases can only be inferred.

One bar Pt-loop experiments were performed by Mo and Carmichael (1985) on the lava composition shown in Table 1. Experimental run temperatures and oxygen fugacities are reported in Table 2. These conditions generally coincide with the Ni−NiO oxygen buffer. Calculated equilibrium phase assemblages at these temperatures and oxygen fugacities are reported in Table 2 and Figs.1–4. The experimental liquidus occurs at 1,272° C with the appearance of spinel (chromite); olivine appears at 1,260° C. Plagioclase precipitates at 1,192° C, and both low-Ca pyroxene and augite begin crystallizing at 1,157° C. By 1,140° C about 50–60% of the experimental charge is crystallized with a solid mode substantially dominated by plagioclase (Mo and Carmichael 1985). Table 2 and Fig. 1 illustrates the agreement between the calculated crystallization history and the experimental results. The calculated points in Fig. 1 are connected by straight lines to give some measure of crystal-

Table 1. Analysis of basaltic andesite studied by Mo and Carmichael (1985)

	Sample Jor 44 (wt %)		Sample Jor 44 (wt %)
SiO_2	52.10	MgO	9.29
TiO_2	0.81	CaO	8.46
Al_2O_3	16.44	Na_2O	3.47
Fe_2O_3	1.56	K_2O	0.74
FeO	6.05	P_2O_5	0.10
MnO	0.14		

Table 2. One bar, equilibrium crystallization, of a basaltic andesite, Jorullo Volcano, Mexico

T (°C)	$\log f_{O_2}$ [a]	Grams precipitated/100 g liquid				$G^{equilibrium} - G^{metastable\ liquid}$ (ΔG in cals)	Undercooling (°C)
		ol	plag	cpx	total		
1,254	−7.01	1.55 [b]			1.55	− 17.44	15
1,227	−7.28	3.99			3.99	− 53.24	42
1,185	−7.74	9.62	11.04		20.66	−164.06	84
1,175	−7.86	11.53	17.38		28.91	−213.86	94
1,165	−7.98	13.25	23.18		36.43	−267.64	104
1,150	−8.16	15.48	30.60	0.03	46.11	−352.91	119
1,140	−8.28	16.81	37.13	3.69	57.63	−449.29	129

$\Delta G = -10.68$ (grams ol) − 5.75 (grams plag) − 15.33 (grams cpx)

[a] Ni−NiO oxygen buffer

[b] Olivine liquidus ~1,269° C

mode volume %   olivine mole % Fo   plagioclase mole % An

1250

1230

1210

1190   liquid

1170

1150   ol   plag

         cpx

20   40   60   80   100 90   80   70 70   60   50
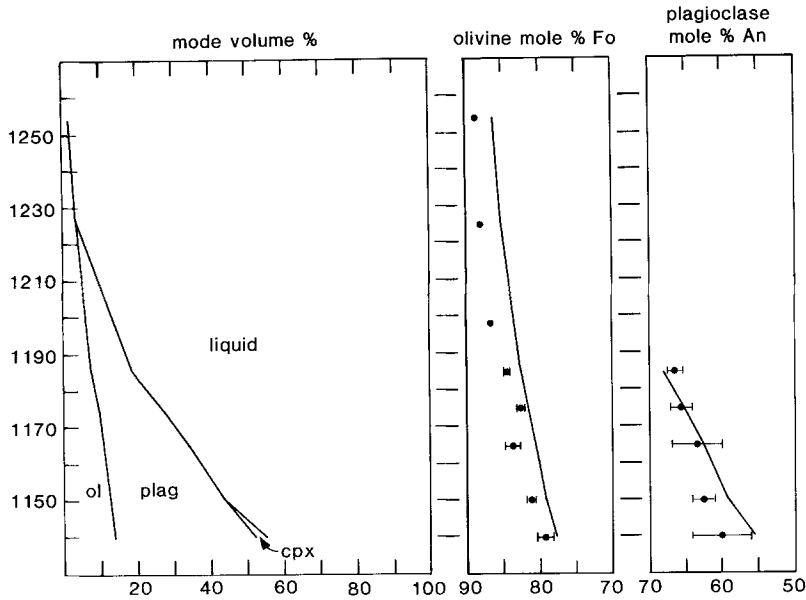
Fig. 1. Calculated mineral proportions and olivine and plagioclase compositions for the equilibrium crystallization of a basaltic andesite (JOR 44, Table 1). The ordinate is labeled in °C. Calculations were performed at 1,254°, 1,227°, 1,185°, 1,175°, 1,165°, 1,150°, and 1,140° C along an oxygen buffer approximating Ni—NiO at 1 bar. Solid lines link the results obtained at each temperature. The experimental phase equilibrium data of Mo and Carmichael (1985) are plotted as solid circles. Brackets indicate $+/-$ two standard deviations reported by these authors

Di   Hd

En   Fs
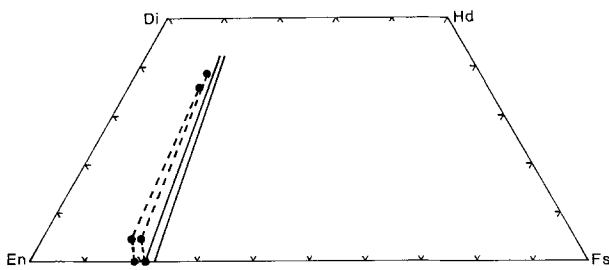
Fig. 2. Calculated coexisting olivine and clinopyroxene compositions for the equilibrium crystallization of a basaltic andesite (JOR 44, Table 1) along the Ni—NiO buffer at 1,150° and 1,140° C and at 1 bar. Solid lines connect the calculated compositions. Experimental data for coexisting clinopyroxene, orthopyroxene and olivine, reported by Mo and Carmichael (1985) as forming at the same two temperatures, are plotted as solid circles. The diagram is in mole %

lization continuity. As can be seen in Fig. 1, the modelled olivine compositions tend to be about 2 mole % more fayalitic than the experimentally determined values while the measured An-contents of the plagioclase seem to define a compositional trend which does not become as albitic as the calculated trend with decreasing temperature. Calculated clinopyroxene compositions at 1,150° C and 1,140° C are displayed in Fig. 2 and are compared with experimentally determined compositions of augite, low-Ca pyroxene and olivine. It should be borne in mind that the modelled pyroxenes are Al-free (see Appendix, Part I) whereas the compositions of the experimental ones have been projected into the quadrilateral. The absence of orthopyroxene in the calculated phase assemblages at these lower temperatures arises from modelling this phase as an enstatite-ferrosilite solid solution. The calculated saturation index, Σ_ϕ, in the residual liquids for this binary solution is 0.97 at

FeO_T

Na_2O
$+K_2O$ MgO
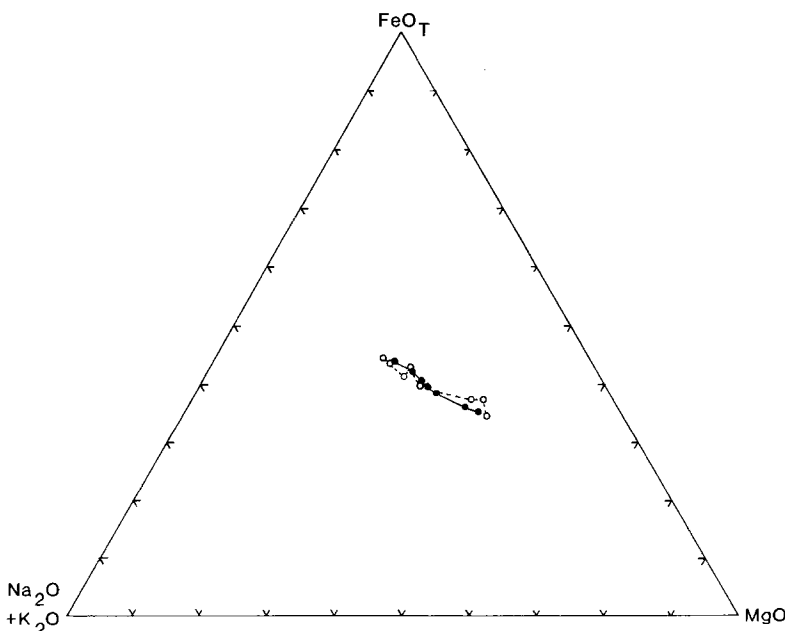
Fig. 3. Calculated liquid path for the equilibrium crystallization of a basaltic andesite (JOR 44, Table 1) along the Ni—NiO oxygen buffer at 1 bar. Solid lines link the calculated results obtained at 1,254° C (*lower right*), 1,227°, 1,185°, 1,175°, 1,165°, 1,150°, and 1,140° C (*upper left*). Corresponding experimentally determined liquid compositions (Mo and Carmichael 1985) are joined by dotted lines. FeO_T is the total iron, expressed as FeO, in the liquid. The diagram is in wt %
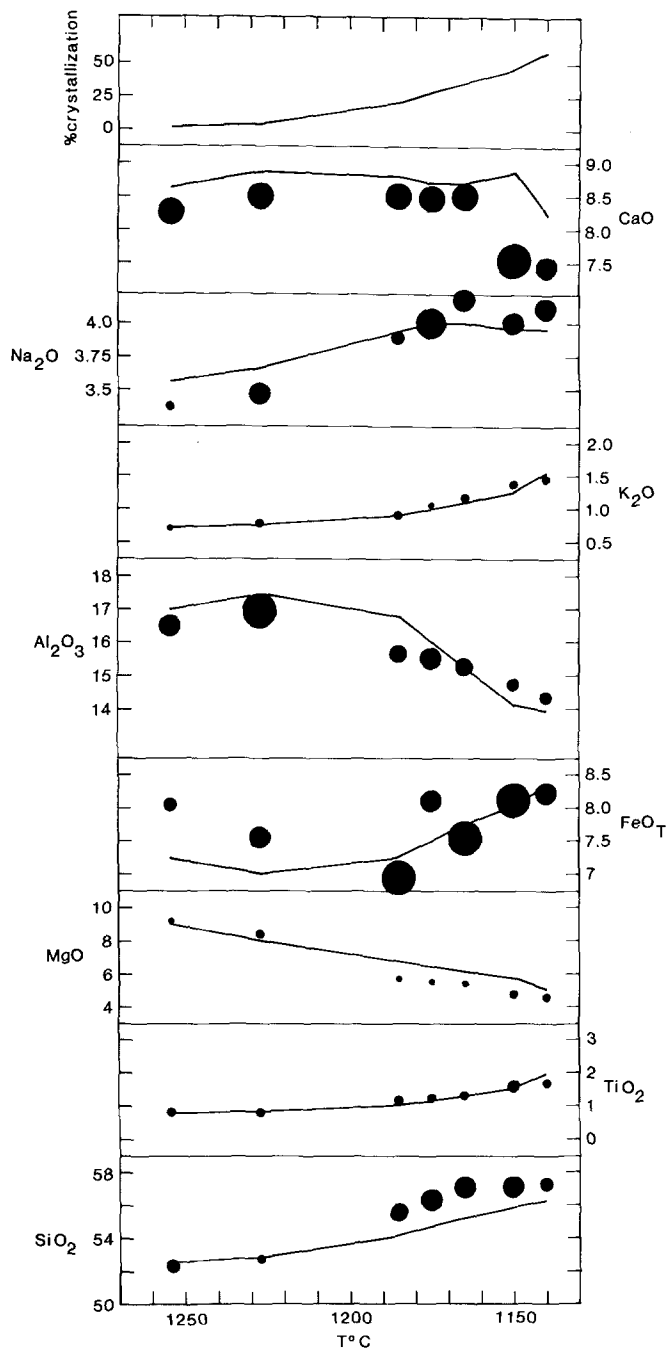
Fig. 4. Calculated liquid compositions for the equilibrium crystallization of a basaltic andesite (JOR 44, Table 1) along the Ni – NiO oxygen buffer at 1 bar. Solid lines link the calculated results obtained at the temperatures indicated in the legend of Fig. 1. Experimentally determined liquid compositions are indicated by solid circles (Mo and Carmichael 1985). The radius of each circle is two reported standard deviations. Note changes in scaling of the y-axis. All compositional data are reported in wt %. FeO$_T$ denotes the total iron, expressed as FeO, in the liquid

1,150° C and 0.99 at 1,140° C indicating that the orthopyroxene is just barely undersaturated (see Part I and Ghiorso et al. 1983). Clearly, if the Ca-bearing orthopyroxene component could be included in these calculations, the saturation index would exceed unity at the more elevated temperatures coincident with clinopyroxene saturation, instead of

below 1,140° C. The modelled composition of the orthopyroxene that saturates just below 1,140° C is En$_{78.2}$. The augite phenocrysts found in the Jorullo lava have compositions which would plot near En$_{45.5}$Fs$_{10.8}$Wo$_{43.8}$, about 2 mole % to the left of the calculated points in Fig. 2. These *phenocryst* compositions suggest that the *experimental* clinopyroxenes may have crystallized metastably inside the solvus. In contrast, Jorullo phenocryst olivine (Fo$_{84.9}$ – Fo$_{88.3}$) and plagioclase (An$_{67.3}$Ab$_{31.8}$Or$_{0.7}$) compositions agree quite well with the higher temperature experimental results (Mo and Carmichael 1985).

The modelled and measured compositions of the residual liquids are displayed in Figs. 3 and 4. Calculated and observed trends on the AFM diagram are almost coincident. The largest inconsistency in the liquid cooling curves of Fig. 4 is in the data for CaO. That the calculated residual liquids are too rich in CaO at 1,140° C and 1,150° C may be a consequence of the fact that the experimentally determined plagioclase compositions at these two temperatures are more anorthitic than those calculated. It should be noted, however, that the final soda concentrations are not substantially higher than the calculated values and the calculated alumina numbers are smaller (!) instead of larger than the experimental results. This apparent inconsistency may be due to Na-loss during the very long experiments (up to 300 h) at lower temperatures (1,140–1,150° C). The experimental MgO trend in Fig. 4 is consistent with the production of a slightly more forsteritic olivine than calculated, but this is not corroborated by the trend for total iron (FeO$_T$).

Overall, the modelled residual liquid and solid compositions, and mineral/melt proportions, reasonably reproduce the experimental data over a cooling interval where 50% of the melt crystallizes. Considering the approximations made in determining pyroxene compositions and our inability to model the precipitation of Cr-rich spinel (Part I, Appendix 1), this observation is all the more interesting. In comparing the calculated equilibrium crystallization model to the Jorullo data we have also tacitly assumed that these experimental results are consistent with the original experimental database of Ghiorso et al. (1983). Any systematic inconsistency will of course be manifest in the results we have presented.

The Jorullo crystallization example provides an interesting case for discussing the Gibbs free energy of crystallization of a typical basaltic lava. In Table 2 we have tabulated this quantity at each temperature as the Gibbs free energy of the equilibrium solid-liquid assemblage minus the Gibbs free energy of a metastable liquid of equivalent bulk composition. The values of ΔG (reported in calories per 100 g of starting material) become increasingly negative as the temperature drops, indicating the greater stability of the heterogeneous assemblage. The important feature to be noticed is the small magnitude of ΔG, which is always less than 500 cals (in absolute value), despite the fact that by 1,140° C over 50 g of solids have crystallized. By way of comparison, the calculated total Gibbs free energy of the system is about −400 kcals over this temperature range. The small free energy of crystallization is significant in that ΔG is just the negative of the chemical affinity, or driving force, of the net crystallization reaction. Because $-\Delta G$ is one to two orders of magnitude smaller than the product of the gas constant, R, and the absolute temperature, T, the rate of continuous crystal growth (Dowty 1980) will

be essentially proportional to the chemical affinity.[2] Consequently, this growth rate will depend on liquid composition according to the stoichiometry of the crystallization reaction. Reaction kinetics of this sort are normally referred to as affinity controlled (Aagaard and Helgeson 1982) and are generally used to describe rate laws in systems "close" to thermodynamic equilibrium. These rate laws necessarily display a quite sensitive dependence of overall reaction rate on liquid composition.

Another interesting feature of the small free energy changes listed in Table 2 is that they are of the same order of magnitude as the activation energies for transport and nucleation in the melt. For example, the surface free energy associated with one gram of nucleii of radius r and solid density ρ dispersed in a melt of surface tension σ is: $[(1/\rho)/(4/3 \pi r^3)] \cdot 4 \pi r^2 \sigma$. If we take σ to be 275 dyne/cm (typical basalt at 1,200° C, Carmichael et al. 1974), ρ to be 3.0 grams/cm^3, and r to be 65Å, the surface energy is about 10 cals (per gram of nucleii). This is the average crystallization energy per gram for the three phases listed in Table 2.

Lastly, it should be remarked that the calculated crystallization free energies are of the order of magnitude of the uncertainties in the thermodynamic data which comprise the crystallization model. These ΔG's are in fact about an order of magnitude smaller than the free energies of mixing for most of the solutions considered as potential solid phases (Part I, Appendix 1).

It follows from these observations that the success of the calculational scheme demonstrated here is due almost entirely to the generation of an internally consistent set of thermodynamic data for silicate liquids (Ghiorso et al. 1983) from which one can resolve free energy differences on the order of tens of calories. This may seem like a rather extraordinary claim, but the apparent success in calculating the correct liquidus temperatures of olivine, plagioclase and clinopyroxene in the Jorullo lava, along with the correct compositions of these minerals (with at most a 5 mole % error), in light of the small free energy changes involved, demonstrates this resolution.

Fractional crystallization of an olivine tholeiite

In this example we are primarily interested in calculating the compositional effects in the solid and liquid phases produced by extreme degrees of crystallization (95% or higher) under conditions approximating perfect fractionation. Consequently, it is not possible to verify completely the results of these calculations by utilizing available experimental data. However, sequences of lavas produced from evolving magma chambers associated with volcanic complexes often show gradational compositions and trends which have been interpreted as extreme examples of crystal fractionation of a basic parental magma. Perhaps the best known of these

2 The rate of continuous crystal growth can be written [Dowty 1980, Eq. (21)]:

rate $\propto D[1 - \exp(-A/RT)]$

where D is the diffusivity (related to the transport of material to the crystal/liquid interface), and A is the affinity. If $A/(RT) \ll 1$, then

rate $\propto D[1 - (1 - A/RT)]$

rate $\propto (D/RT)A$

Table 3. Initial composition of olivine tholeiitic liquid (wt %)

	Analyzed composition (H. 128, Carmichael 1964a)	Composition used in calculations
SiO$_2$	47.07	48.47
TiO$_2$	1.66	1.71
Al$_2$O$_3$	14.86	15.31
Fe$_2$O$_3$	4.08	1.66[a]
FeO	7.20	9.90[a]
MnO	0.17	_[b]
MgO	8.52	8.77
CaO	11.47	11.57
Na$_2$O	2.24	2.30
K$_2$O	0.20	0.20
P$_2$O$_5$	0.18	_[c]
H$_2$O$^+$	1.32	0.10[d]
H$_2$O$^-$	0.93	_[d]
Total	99.90	[100.00]

[a] The ferric/ferrous ratio was set by the QFM oxygen buffer at 1,200° C according to the equations of Myers and Eugster (1983) and Kilinc et al. (1983). The original ferric/ferrous ratio in the rock has been upset by subsequent oxidation and is not representative of magmatic conditions

[b] MnO normally enters olivines and pyroxenes as the liquid crystallizes. As this is not possible using the current thermodynamic dataset (Part I, Appendix 1) to avoid building up large concentrations of MnO in highly fractionated residual liquids its concentration was neglected at the onset

[c] The Thingmuli lavas of basaltic andesite and icelandite composition contain microphenocrysts of apatite. As the crystallization of this phase cannot be modelled using the current thermodynamic dataset (Part I, Appendix 1) to avoid building up large concentrations of P$_2$O$_5$ in highly fractionated residual liquids its concentration was neglected at the onset

[d] The high water content of this olivine tholeiite is due to low-temperature alteration. A value of 0.10 wt % was selected for calculational purposes in order to produce a reasonable water content (2.00 wt %) in a residual rhyolitic liquid expected to form after about 95% crystallization (Carmichael 1964a). Though water does not enter into the solid phases its presence is necessary to suppress the solidus of the most highly fractionated lavas

volcanic centers is Thingmuli in Eastern Iceland (Carmichael 1964a, 1967a). The lavas of this Tertiary volcano range in composition from olivine tholeiites through tholeiites, basaltic andesites and icelandites to rhyolites. They are interpreted (Carmichael 1964a) as having been derived by periodic eruption of a shallow magma chamber undergoing crystal fractionation. Because of the detailed information available on the mineralogy and petrology of the Thingmuli lavas, we have chosen the most "primitive" representative of this suite as the initial bulk composition for our fractionation example (Table 3). If the composition of this olivine tholeiite is at all a reasonable approximation for the parental magmatic liquid at an early stage in the crystallization history of the Thingmuli magma, then subsequent crystal fractionation of this liquid should give rise to the more evolved lavas in the series. Therefore, under this assumption, the success of the modelled fractionation sequence produced from the liquid of Table 3 can be judged against petrographic and analytical data obtained from the rocks directly. Although this comparison has considerable appeal, the assumption upon which it is based should al-

ways be borne in mind in considering the results presented below.

Initial liquid

The first difficulty encountered in performing fractionation calculations on the Thingmuli tholeiite concerns describing the oxidation state of the initial liquid, since alteration has destroyed the primary ferric/ferrous ratio in the erupted lava. Two indirect lines of evidence, however, suggest that the Thingmuli magma evolved essentially along the QFM buffer. Application of the Fe–Ti oxide geothermometer of Buddington and Lindsley (1964), using compositions of coexisting homogeneous-spinels and ilmenites from the Thingmuli lavas, yields $T-f_{O_2}$ coordinates which define a trend (for the entire fractionation series) about 0.2 log units below QFM (Carmichael 1967a). In addition, liquidus calculations described by Ghiorso et al. (1983) on the olivine tholeiitic lavas of Thingmuli demonstrate that calculated initial olivine compositions match those of phenocryst cores exactly, when the ferric/ferrous ratio of the liquid is set according to the QFM buffer. Such calculations are sensitive enough to discriminate easily $+/-0.5$ log units in f_{O_2} at a given temperature and are thus consistent with oxygen fugacities inferred from the coexisting Fe–Ti oxides. In light of these arguments the initial f_{O_2}, and hence the liquid ferric/ferrous ratio in Table 3, are assigned values consistent with the QFM buffer at a temperature corresponding to the first appearance of olivine.

The role of oxygen fugacity and the path of crystallization

As the oxygen fugacity of the Thingmuli magma appears to evolve along a $\log f_{O_2} - T$ path coincident with the QFM buffer, a brief consideration of the observed crystallization sequence (olivine, plagioclase, augite, spinel) indicates that during the initial stages of iron-enrichment the crystallizing magma must be continuously reducing ferric to ferrous iron to remain on this "buffer". This chemical exchange can be viewed as a transfer of oxygen from the ferric iron component in the liquid to some other oxygen reservoir internal or external to the system. That this transfer is necessary can be easily demonstrated from arguments outlined in Part I, namely, that crystallization along an f_{O_2} buffer implies a nearly constant ratio of ferric/total iron in the residual liquid. Clearly, if FeO is removed from this liquid by precipitation of olivine and augite, the ferric/total iron ratio in the melt will increase unless ferric is reduced to ferrous iron. In the latter stages of crystallization, once spinel dominates the sequence and iron enrichment ceases, the amount of Fe_2O_3 relative to FeO that is removed from the liquid will depend upon spinel composition (see below) and iron must either be reduced or oxidized by the system in order to maintain fractional crystallization along the observed $\log f_{O_2} - T$ path. There are two possible sources and sinks for the oxygen which participates in the iron redox equilibria described above. The first can be thought of as a magmatic oxygen reservoir composed of melt species capable of undergoing oxidation-reduction equilibria. These species might include dissolved sulfur (Carmichael and Ghiorso 1985) and carbon gases and transition elements other than iron. The second oxygen reservoir might possibly be the country rock surrounding the magma chamber. In this latter case the mechanism of oxygen exchange between magma

chamber and surroundings is probably one of hydrogen diffusion (Sato 1978; Arculus and DeLano 1981); the fugacity of hydrogen being linked to that of oxygen through the breakdown of water. Hydrogen diffusion is rapid enough, when compared to other metasomatic processes, to make this mechanism of open system oxygen transfer petrologically relevant. Irrespective of the actual oxidation-reduction mechanisms which operate in nature, for calculational purposes the crystal fractionation of the Thingmuli olivine tholeiite must be viewed as an open system process. This is a consequence of expressing the composition of a magmatic system using thermodynamic components which include only an iron redox-couple (Ghiorso et al. 1983; Part I). Thus, whether the iron redox state is maintained by homogeneous equilibria involving species other than iron or by oxygen metasomatism is not crucial to *calculating* the crystallization sequence. For *calculational* purposes we need only consider the oxygen fugacity of the magma to be fixed by some "external redox equilibria" and model a net chemical exchange of oxygen across the boundaries of our compositionally restricted system. Upon reflection it can be seen that this model simply treats oxygen as a perfectly mobile component (Korzhinskii 1959). Fractionation calculations in such an "open magmatic system" can be performed in a straight-forward manner (Part I) as they are based upon the thermodynamic treatment of such systems provided by Korzhinskii (1959) and Thompson (1970). In the subsequent discussion we will make considerable use of "open system modelling" of the crystal fractionation process. It is important to keep in mind that our inability to completely characterize all of the redox equilibria in the liquid necessitates this approach. It is most likely that in nature both hydrogen metasomatism and homogeneous redox equilibria control the oxygen fugacity of a crystallizing magma. We will not attempt here to assess the relative importance of either mechanism, but we do suggest that one or both must be important during the fractional crystallization of any tholeiitic magma which undergoes iron enrichment.

Results of the calculation

Results of the calculation of the open system fractional crystallization of the Thingmuli olivine tholeiite are shown in Fig. 5 and subsequent figures. The fractionation interval was taken to be 15° C, that is the system was dropped in temperature at 15° C increments, the equilibrium solid/liquid assemblage determined at each T, and the solids withdrawn before the next step. Smaller fractionation intervals had no effect upon the solid/liquid compositions produced at any advanced step. We take these calculations, therefore, to closely represent perfect fractionation. The crystallization sequence inferred from the Thingmuli lavas is duplicated very well by the 1 bar calculations displayed in Fig. 5. The natural crystallization sequence is (Carmichael 1964a) olivine, plagioclase, augite, spinel (Fe–Ti oxide), then olivine-out replaced by pigeonite with essentially the simultaneous appearance of minor amounts of ilmenite. Apatite crystallizes from the basaltic andesites and icelandites and fayalitic olivine returns in the icelandites, replacing Ca-poor pyroxene in the more acid rocks. Only one feldspar is ever produced by the Thingmuli lavas and this is zoned to an anorthoclase in some of the granophyres associated with (and genetically related to) the sequence. In addition, the
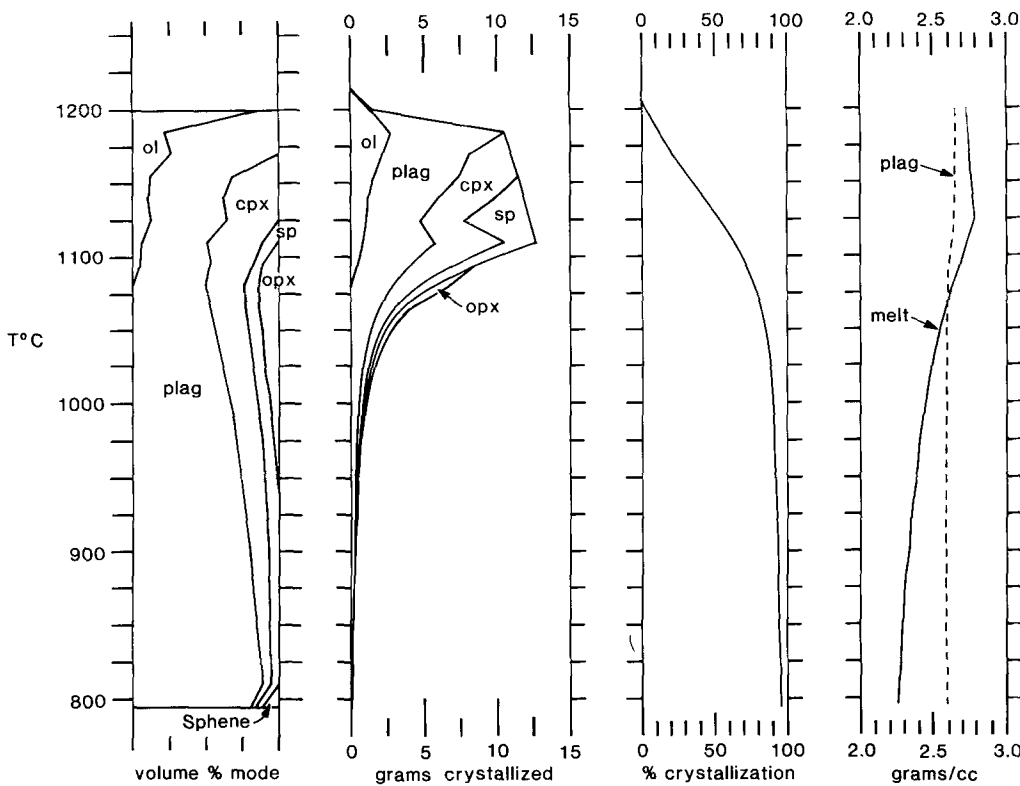
Fig. 5. Calculated mineral proportions and melt and plagioclase densities for the fractional crystallization of an olivine tholeiite (Carmichael 1964a) along the QFM buffer at 1 bar. Crystallization was incremented in 15° C intervals. Results at each temperature are connected by continuous lines. *Far left*: Mineral mode during each interval in the crystallization history. *Middle left*: Mass of material solidified during each interval of the crystallization history. Initial liquid mass was 100 g. *Middle right*: Cumulative % of liquid solidified (may be read directly in grams). *Far right*: Density of plagioclase and melt formed during each interval of the crystallization history. Note that in excess of 80% of the melt must crystallize before the plagioclase becomes more dense than the coexisting liquid. *ol*, olivine; *plag*, plagioclase; *cpx*, clinopyroxene; *sp*, ulvöspinel-magnetite solid-solution; *opx*, orthopyroxene

granophyres contain magnetite phenocrysts shrouded by sphene. With the exception of ilmenite and apatite, which were suppressed from the calculation due to inadequate thermodynamic data or inappropriate liquid activity/composition relations (Appendix, Part I), the only glaring inconsistency in the calculated crystallization sequence concerns the disappearance of orthopyroxene without the reappearance of an iron-rich olivine. Most likely this is due to a failure in the liquid activity model (Ghiorso et al. 1983) to correctly predict olivine-liquid equilibria in hydrous-, acidic-melts. Additionally, it should be borne in mind that the calculated pyroxene compositions are represented completely within the quadrilateral, and a Ca-absent orthopyroxene (opx) is taken as a proxy for pigeonite in Fig. 5. The cumulative phase proportions for the entire fractionation calculation at 1 bar are summarized in Table 4.

Figure 5 shows that the vast majority of crystallization takes place in the first 100° C. The calculated solid mode in this early stage is dominated by plagioclase with subordinate augite. This is corroborated by petrographic examination of the tholeiites of the Thingmuli series (Carmichael 1964a). The more evolved lavas largely contain plagioclase phenocrysts and this is also inferred by the calculations shown here. The spike of spinel precipitation at 1,125° C is reflected in the large numbers of Fe−Ti oxide phenocrysts found in the more evolved tholeiites and the preponderance of magnetite-rich glass which dominates the groundmass of these lavas (Carmichael 1967a). During the

Table 4. Thingmuli fractionation results at 795° C

Phase	Grams	Volume (cc)	% total volume of solids
Olivine	12.04	3.60	11
Sphene	0.03	0.01	0
Orthopyroxene	2.43	0.73	2
Clinopyroxene	24.58	7.44	23
Plagioclase	48.99	18.58	59
Spinel	6.98	1.44	5
Liquid	4.40	1.94	

whole of the first 80% of crystallization, the calculated density of the precipitated plagioclase is less than that of the liquid (Fig. 5). This would suggest that crystal sorting could operate effectively in the Thingmuli magma chamber to produce "anorthositic" or plagioclase porphyritic rocks in its upper levels. Plagioclase and olivine porphyritic basalts and plagioclase cumulate boulders associated with acid pyroclastics erupted from the Thingmuli volcanic center (Carmichael 1964a) substantiate the implication that plagioclase floatation and olivine sinking were both active processes in the evolution of the Thingmuli magma. It should be noted that the *decrease* (at 1,120° C) in calculated liquid density shown in Fig. 5 is related to the precipitation of spinel. The spinel phase does not replace olivine on the
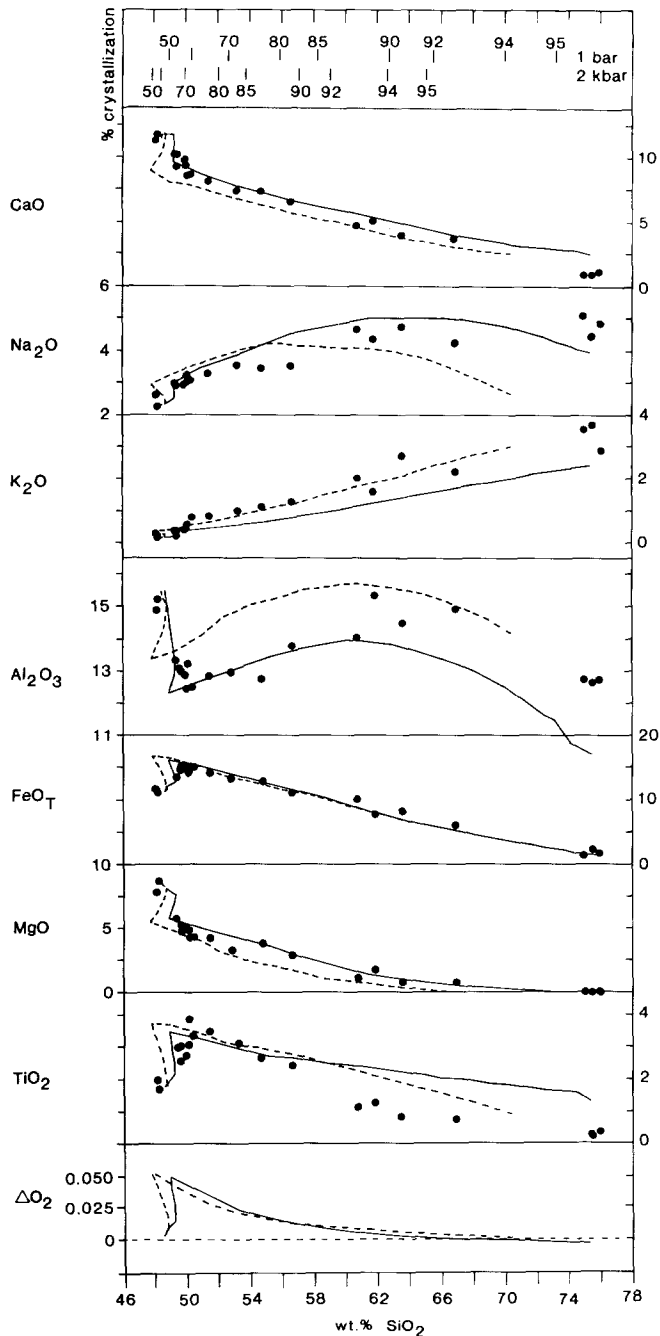
Fig. 6. Calculated liquid variation diagram for the fractional crystallization of an olivine tholeiite (Carmichael 1964a) along the QFM buffer at 1 bar (results at each temperature connected by continuous solid lines) and two kilobars (results at each temperature connected by continuous dotted lines). Crystallization was incremented in 15° C intervals. The % crystallization as a function of silica content is indicated at the top of the diagram. At the bottom, the cumulative amount of assimilated ($+$) or expelled ($-$) oxygen is reported as a function of wt % SiO_2 in the melt. All compositional units are in wt %. ΔO_2 is reported in grams and should be referenced to 100 g of initial liquid. Note changing scale of the ordinate. Solid circles denote data on the Thingmuli fractionation series taken from Carmichael (1964a)

liquidus, as was suggested as a possible reaction relationship by Carmichael (1964a); olivine disappears at least 50° C below the first appearance of spinel due to its replacement by orthopyroxene on the liquidus.

The highest Fe—Ti oxide temperature obtained on the Thingmuli lavas is 1,080° C (Carmichael 1967a). It was derived from ilmenite and homogeneous-spinel in the more primitive tholeiites. If the appearance of ilmenite and pigeonite roughly coincide, then this temperature is consistent with the calculated appearance temperature of orthopyroxene indicated in Fig. 5.

Variation diagrams of residual liquids produced from fractionation calculations at 1 bar and 2 kbars are shown in Fig. 6. Compositions of the Thingmuli lavas reported by Carmichael (1964a, Table 9) are plotted for comparison. Percent crystallization is indicated at the top of the figure and cumulative oxygen (grams of O_2 per 100 grams of magma) released ($+$) or absorbed ($-$) by the system is indicated at the base. Bearing in mind our assumption that the composition of the most primitive olivine tholeiite is unaffected by crystal sorting and represents the initial Thingmuli magma composition, the correspondence shown in Fig. 6 is remarkable. This is particularly so when one considers the extreme degrees of crystal fractionation involved. For example, a 0.05 wt % error in the determination of any oxide in the composition of the olivine tholeiite could magnify itself into a 1.00 wt % error in the derived residual liquid at 95% crystallization.

The majority of the natural compositions plotted in Fig. 6 are bracketed by the one bar and two kilobar curves. This would suggest that the Thingmuli magma chamber differentiated at a fairly shallow depth. Where the calculated curves in Fig. 6 dramatically depart from the natural trends the discrepancy can usually be ascribed to the precipitation of a phase slightly off composition (see below) or the suppression of a phase known to form in the sequence. In the case of TiO_2 the suppression of ilmenite probably accounts for the high titania values in the residual liquids.

Figure 6 clearly shows the initial increase and subsequent decrease in silica concentration which is characteristic of fractionating tholeiitic liquids. The turnover to higher silica contents, which is accentuated by sharp breaks in all the variation curves, denotes the first appearance of spinel on the liquidus. Prior to this event the distinctly negative slopes of the curves shown in Fig. 6 reflect the precipitation of clinopyroxene. The initial positive slopes, of course, express the crystallization of olivine and plagioclase.

Additional insight into the affects of pressure and oxygen fugacity on the compositions of the calculated residual liquids can be gained by examining Figs. 7a and b. These figures are also convenient for discussing the general effects of oxygen exchange during magmatic crystallization. It is generally accepted (e.g. Osborn 1959, 1962; Yoder and Tilley 1962) that a tholeiitic magma crystallizing at constant bulk composition will generate an extreme iron-enrichment trend on an AFM diagram depicting the compositions of its derived liquids. Such a trend is known as the Fenner trend and is characteristic of large, apparently closed, intrusive systems such as the Skaergaard (Wager and Brown 1967). In contradistinction, if the magmatic system is presumed to be open to oxygen, in particular if the partial pressure of oxygen is maintained at a constant value[3] during the crystallization event, fractional crystallization of a tholeiitic liquid is presumed to generate a residuum rich

3 It should be noted that a constant partial pressure of oxygen (i.e. ~constant fugacity) implies "oxidation" of the magma as the temperature drops. For instance: the oxygen fugacity that corresponds to the QFM buffer at 1,200° C is roughly identical to that of the magnetite-hematite buffer at 820° C

a

b
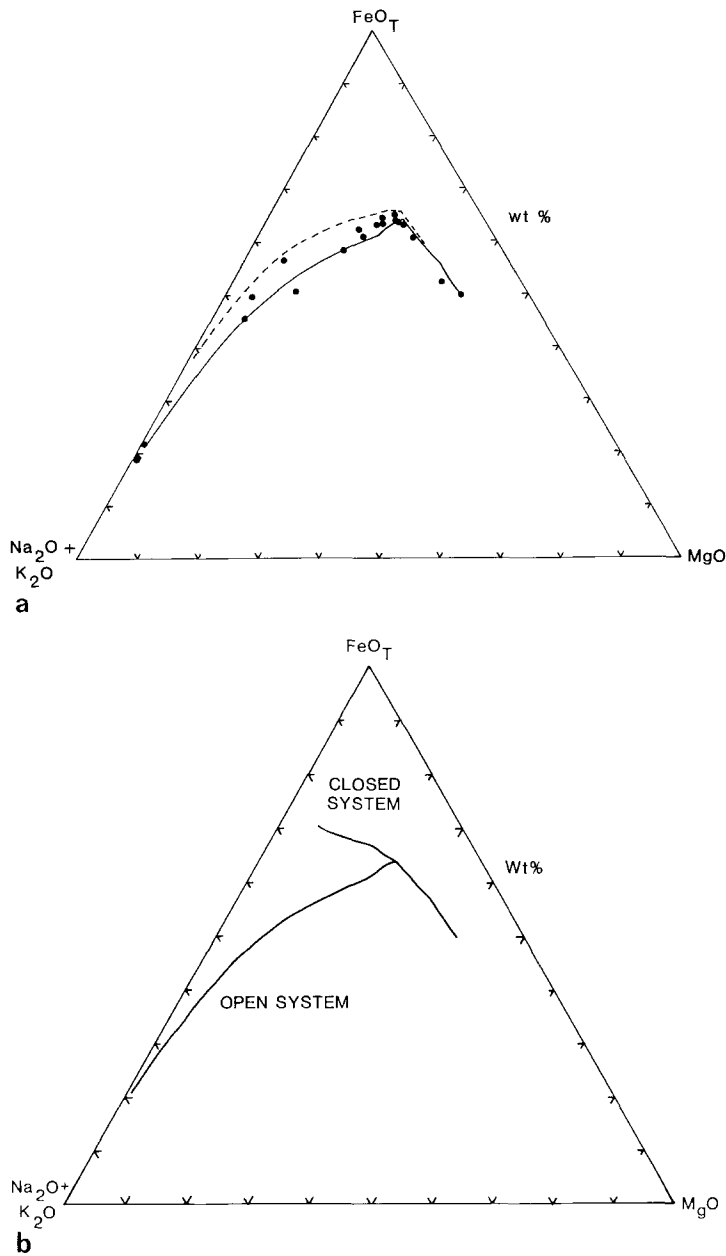
Fig. 7a, b. Calculated liquid path for the fractional crystallization of an olivine tholeiite (Carmichael 1964a). Crystallization was incremented in 15° C intervals. The diagrams are in wt % oxides. FeO_T denotes total iron expressed as FeO. **a** Calculations performed along the QFM buffer at 1 bar (results at each temperature connected by continuous solid lines) and two kilobars (results at each temperature connected by continuous dotted lines). Solid circles denote data on the Thingmuli fractionation series taken from Carmichael (1964a). **b** Calculations performed at 1 bar along the QFM buffer (labeled OPEN SYSTEM) and in a system closed to oxygen exchange (labeled CLOSED SYSTEM)

in alkalies and silica and low in iron, i.e., the Bowen trend. In the latter case, the rapid initial depletion in total iron is due to the oxidation of ferrous to ferric iron and the precipitation of large quantities of spinel.

In the fractionation calculation displayed in Figs. 5 and 6, the net change in the oxygen content of the system is essentially zero[4] but the absolute amount of oxygen transfered in and out of the magma is quite large (see Table 5). The point at which the direction of transfer is reversed corresponds to the apex of the iron-enrichment curve shown in Fig. 7a. To explore the relationship of our "buffered" fractionation calculations to the classical trends of Fenner and Bowen, we have calculated the phase compositions and proportions associated with the fractional crystallization of the olivine tholeiite of Table 3 at *constant bulk composition* (constant amounts of both ferrous and ferric iron). In terms

---

4 There is a small net increase in oxygen content during crystallization. This effect was anticipated for open system basalt fractionation by Osborn (1959)

Table 5. Thingmuli fractionation: oxygen production and consumption

	Initial liquid (grams)	1,125° C liquid + Σ (fractionated solids) (grams)	Final liquid + Σ (fractionated solids) (grams)
Fe_2O_3	1.65	1.16	1.68
FeO	9.84	10.28	9.82
O_2		0.04890	−0.00321

of the AFM diagram of Fig. 7b the residual liquids from this 1 bar calculation follow the "buffered" trend quite closely up to the iron enrichment apex, all the while crystallizing olivine, plagioclase and clinopyroxene and generating melt oxygen fugacities which rise slightly above the QFM buffer (a maximum of about 0.6 log units). Once spinel begins to precipitate, however, the closed system path departs rapidly from that of the buffered system. Coincident

Table 6. Closed system fractionation of the Thingmuli olivine tholeiite

T (°C)	wt % Ratio of Fe_2O_3/FeO in residual liquid	Melt $\log f_{O_2}$	QFM buffer $\log f_{O_2}$
ol+plag			
1,200	0.1731	−8.27	−8.30
1,185	0.1822	−8.40	−8.47
1,170	0.1916	−8.54	−8.65
ol+plag+cpx			
1,155	0.2170	−8.52	−8.82
1,140	0.2464	−8.50	−9.01
1,125	0.2834	−8.46	−9.19
ol+plag+cpx+spinel			
1,110	0.3612	−8.19	−9.38
1,095	0.5917	−7.46	−9.57

$(1+x)FeO + x\,TiO_2 + (1-x)\,Fe_2O_3$
$= (1-x)\,Fe_3O_4 + x\,Fe_2TiO_4$ $Fe^{++}_{1+x}\,Fe^{+++}_{1-x}\,Ti_xO_4$

Mole fraction ulvöspinel (x) in product	wt % ratio of Fe_2O_3/FeO in reactants
1.00	0.0
0.85	0.0365
0.75	0.0643
0.65	0.0954
0.55	0.1306
0.45	0.1707
0.35	0.2166
0.25	0.2699
0.15	0.3325
0.00	0.4499

with the precipitation of spinel the oxygen fugacity of the melt rises sharply as the Fe_2O_3/FeO ratio in the liquid increases (Table 6). This is due to the fact that the liquid saturates with a spinel of composition $\sim Uv_{75}$. As can be deduced from the calculations reported in Table 6, precipitation of this spinel withdraws oxidized and reduced iron from the melt in a ratio which is about a factor of four less than that available, thus causing the ferric/ferrous ratio of the liquid to increase. The more the oxygen fugacity (in the melt) increases, the greater the tendency that the precipitation of spinel will oxidize the melt. Table 6 shows that at 1,095° C the melt has become so oxidized that even the precipitation of pure magnetite cannot curb the trend toward further oxidation. As these events take place, there develops a tendency to reduce the degree of spinel supersaturation with each temperature decrease, consequently preventing the removal of large amounts of iron from the residual liquid. The net effect is to drive the liquid towards the FeO_T apex in Fig. 7b while simultaneously advancing in composition toward the alkali-iron join. The ultimate result is extreme iron-enrichment, with the liquid ferric/ferrous ratio corresponding closely to the magnetite-hematite buffer. The AFM diagram trend produced from this closed system calculation closely resembles that of Fenner.

In light of the oxidizing effects of spinel crystallization in the closed system, it is intriguing to discuss why the opposite effect occurs in the "open system" or "buffered" calculation. This can easily be understood by writing the crystallization reaction:

$$(1+x)FeO + x\,TiO_2 + \frac{r}{1-2r}(1+x)Fe_2O_3$$
$$\text{liquid} \quad \text{liquid} \quad\quad\quad \text{liquid}$$
$$+ \frac{1}{2}\left[3 - 3x - \frac{3r}{1-2r}(1+x)\right]O_2$$
$$\text{gas}$$
$$= (1-x)Fe_3O_4 + x\,Fe_2TiO_4$$
$$\text{spinel} \quad\quad \text{spinel}$$

where x is the ulvöspinel mole fraction in the precipitated spinel and r is the molar Fe_2O_3/FeO_T ratio in the liquid (fixed by the f_{O_2} buffer). For the Thingmuli olivine tholeiite of Table 3, r is 0.066, and precipitation of any spinel more magnetite rich than Uv_{86} causes oxygen to be consumed in its formation.

Our calculations suggest that generation of the Bowen trend by continous oxidation of the melt (maintenance of a constant oxygen partial pressure as the temperature decreases, e.g. Osborn 1959) is quite feasible in that oxidation will tend to saturate the liquid sooner in a more magnetite rich spinel. The oxygen reservoir will in turn assure that sufficient spinel precipitates to rapidly lower the iron content of the melt and generate an AFM diagram Bowen trend. Although varying cotectic proportions and assimilation of salic material can produce the same effect (Grove and Baker 1984), our calculations demonstrate the importance of oxygen exchange in the fractional crystallization of basaltic magma. These calculations, in turn provide some evidence for the role of oxygen metasomatism in the evolution of the lavas of the Thingmuli series.

If sulfur could be introduced as an additional component in these calculations, the necessity for open system oxygen exchange would be in part alleviated (Carmichael and Ghiorso 1985). Basaltic magmas with more than 500 ppm dissolved sulfur could store any evolved oxygen released prior to spinel precipitation by converting reduced to oxidized sulfur. This oxygen would then be available for consumption at later stages of crystallization. The only restriction on the feasibility of this mechanism is that a sulfur-oxygen f_{O_2}-buffer exist that roughly coincides with QFM – the observed $f_{O_2} - T$ path of the Thingmuli lava series. Carmichael and Ghiorso (1985) have shown that the $S_2 - SO_2$ oxygen buffer essentially follows QFM over the temperature range of interest. They have suggested that this equilibrium accounts for the self-buffering capacity of basaltic magmas during the early stages of their crystallization. Although we might speculate on the significance of other homogeneous equilibria which function as magmatic oxygen reservoirs (e.g. $Mn^{+3} - Mn^{+2}$, $V^{+3} - V^{+2}$, $Cu^{+2} - Cu^{+1}$, etc.), there is presently no data available to judge their relative importance.

In Fig. 7a the effect of pressure on the fractionation trend is quite apparent. This effect results from the tendency of the melt to discard liquid components which raise its free energy at elevated pressure. The liquid components which are preferentially discarded are those with the largest partial molar volumes (Mo et al. 1982). Thus, elevated pressures force the liquid molecule $NaAlSi_3O_8$ ($\bar{v}=112.40$ cm³/mole) to precipitate in preference to $CaAl_2Si_2O_8$ ($\bar{v}=104.18$ cm³/mole), generating a more sodic plagioclase. Similarly, the relative liquid volumes of Mg_2SiO_4 ($\bar{v}=49.39$ cm³/mole) and Fe_2SiO_4 ($\bar{v}=52.61$ cm³/mole) tend to generate a more fayalitic olivine. The effect is accentuated

for the iron-bearing minerals in that the partial molar volume of molten Fe_2O_3 is very large (42.40 cm^3/mole, Mo et al. 1982). The tendency to minimize the free energy of the liquid coupled with crystallization along the f_{O_2} buffer (constant Fe_2O_3/FeO_T ratio) forces the conversion of Fe_2O_3 to FeO and the ferrous iron enrichment of the precipitated mafic phases. The trend in Fig. 7a demonstrates that the relative depletion of the liquid in soda far outweighs that of iron as crystallization proceeds at 2 kbars. This may also be seen in the variation curves of Fig. 6. The apparent iron enrichment in the 2 kbar-derived liquids seen in Fig. 7a over that of the 1 bar calculation is consistent with the fact that the same silica content is not achieved at the same degree of crystallization in both calculations.

Details of the petrological interpretation of Figs. 6 and 7 may be gleaned from Carmichael's (1964a) analysis of the Thingmuli lavas. His interpretation applies well to the *calculated* variation curves. The "problem" posed by Carmichael of the subsequent enrichment of FeO_T in the icelandites and rhyolites can largely be understood in terms of the above discussion of oxygen fugacity as it relates to variation trends. Volumetric considerations aside, our calculations show no need to invoke an independent origin for the acid magma of the Thingmuli complex.

Comparisons between the calculated and measured compositions of solid phases produced during the 1 bar fractional crystallization of the Thingmuli olivine tholeiite are shown in Figs. 8 and 9. As can be seen in Fig. 8, this lava series is characterized by a single feldspar (zoned to anorthoclase in the granophyres) whose calculated composition varies from An_{81} to An_{17} (weighted mean: An_{61}). Calculated olivine compositions are shown in Fig. 9. These vary from Fo_{82} through Fo_{66} (weighted mean: Fo_{66}) which agrees well with the compositions of zoned olivine phenocrysts ($Fo_{83}-Fo_{55}$) from the Thingmuli olivine tholeiite (Carmichael 1976b). The Thingmuli olivines contain rather small amounts of Mn and Ca and are well represented in the Mg−Fe binary.

A coexisting natural olivine-augite pair is indicated in Fig. 9. The tie-line which joins the compositions of these phenocrysts is sub-parallel to the calculated 1 bar olivine-clinopyroxene and orthopyroxene-clinopyroxene tie-lines. The latter are indicated in the figure by solid lines. It is of interest to note that the groundmass pigeonite-augite tie-lines are inconsistent with those of the more magnesian phenocrysts. The Thingmuli augites contain relatively minor amounts of Al_2O_3 (~ 2 wt %), TiO_2 (~ 1 wt %) and Na_2O (~ 0.5 wt %, Carmichael 1967a), which permits their compositions to be adequately approximated by the quadrilateral pyroxenes. Calculated clinopyroxene compositions deviate from the phenocryst trend at higher iron contents and advanced stages of fractionation. The calculated trend, which heads towards wollastonite, may be a reflection of an inadequately modelled Ca-absent orthopyroxene.

The compositions of homogeneous spinels from the Thingmuli lavas determined by Carmichael (1967a) range from Uv_{78} (tholeiites) to Uv_{60} (rhyolite). Calculated compositions over the same interval range from Uv_{68} to Uv_{64} (weighted mean: Uv_{66}).

Consideration of our modelled solid phase compositions for the open system fractionation of the Thingmuli olivine tholeiite reveals excellent agreement with observed mineral phases in the derivative lavas for about the first 85% of crystallization. This is to be expected from the observed
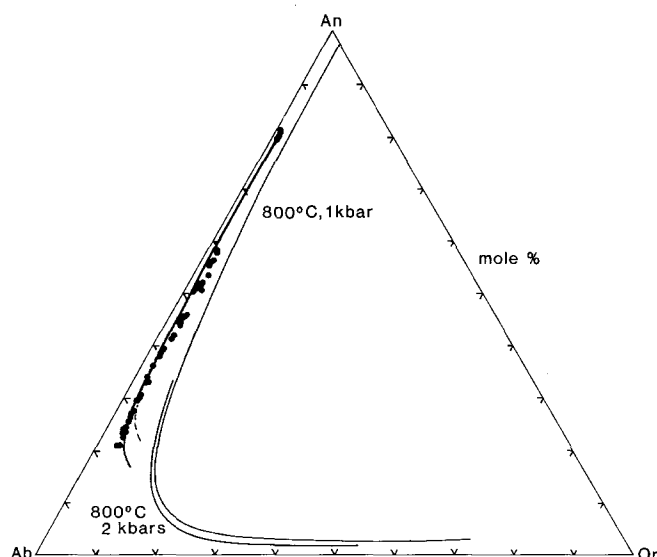
Fig. 8. Calculated compositions of plagioclase precipitated during each interval of the fractional crystallization of an olivine tholeiite (Carmichael 1964a) along the QFM buffer at 1 bar and two kilobars. Crystallization was incremented in 15° C intervals. One bar results are shown connected by a continuous solid line. Two kilobar compositions overlap those computed at 1 bar except near the Ab apex where they are shown connected by a continuous dotted line. Solid circles denote data on plagioclase phenocryst compositions (Carmichael 1967a) from lavas of the Thingmuli fractionation series. The 800° C ternary solvii were computed using the feldspar solution model of Ghiorso (1984). The diagram is in mole %
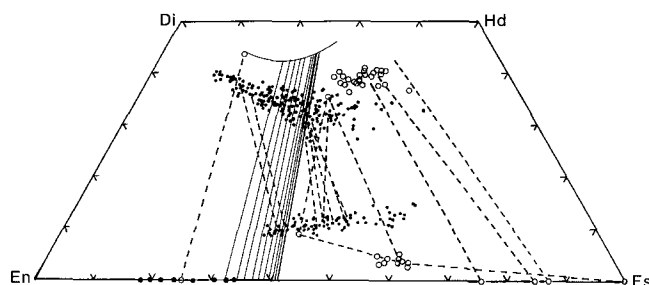
Fig. 9. Calculated compositions of olivine, orthopyroxene and coexisting clinopyroxene precipitated during each interval of the fractional crystallization of an olivine tholeiite (Carmichael 1964a) along the QFM buffer at 1 bar. Crystallization was incremented in 15° C intervals. Successive clinopyroxene compositions are connected by solid lines. Calculated olivine compositions are shown by large solid circles. Tie lines connecting coexisting olivine and clinopyroxene and orthopyroxene and clinopyroxene are also indicated by solid lines. The open circles represent the compositions of phenocrysts of olivine, Ca-poor pyroxene and augite from the lavas of the Thingmuli fractionation series (Carmichael 1967a). The smaller solid circles denote the compositions of groundmass pyroxenes. Coexisting tielines for the natural pairs are dotted. The diagram is in mole %

match of the residual liquid compositions (Figs. 5 through 7), but emphasizes two rather startling general results of this fractionation example: 1) that the Thingmuli lava series itself is related by crystal fractionation with minor chemical variation due to crystal sorting or other processes, and 2) that the calculational scheme of Part I which is based upon the solution model of Ghiorso et al. (1983) can be extrapolated to liquid compositions far removed

X 10 (integral heat)
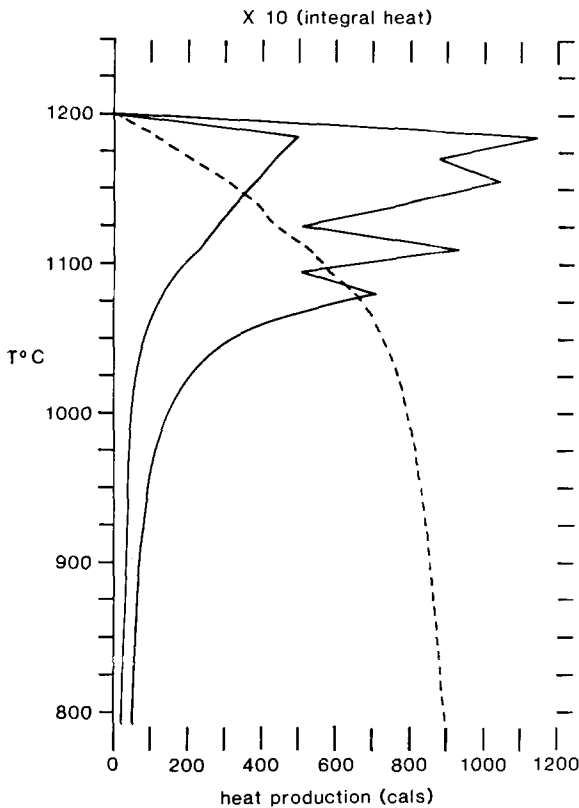
Fig. 10. Calculated heat production due to the fractional crystallization of an olivine tholeiite (Carmichael 1964a) along the QFM buffer at 1 bar. The outer solid curve represents a series of straight line segments connecting calculated values of the heat output produced during each successive 15° C cooling interval. The inner solid curve corresponds to that portion of the heat released purely to cool the system in each interval. The difference between the two curves is the calculated latent heat of fusion. The dotted curve corresponds to the cumulative heat production. It is plotted on an abscissa scaled by a factor of 10. All lines are arbitrarily brought to zero at 1,215° C where the system consists of 100 g of stable liquid

from the original experimental database. In our opinion the success of the Thingmuli calculations is due to the fact that they were performed using sound thermodynamic solution models for the liquid and solid properties and a calculational scheme which verifies the stability of the resulting phase assemblages.

Heat effects of crystallization

Before turning to our final crystallization example it will be useful to examine the behavior of several thermodynamic state functions which characterize the fractionation of the Thingmuli olivine tholeiite. In Fig. 10 the instantaneous and cumulative heats of crystallization are indicated for 100 grams of initial liquid crystallizing, at a pressure of 1 bar, to 95.6% solid. Spikes in the latent heat of crystallization reflect the appearance of new phases on the liquidus. If the rate (dT/dt) at which the magma cooled were directly proportional to the rate at which heat could be removed from the system, then the cumulative curve of Fig. 10 demonstrates that during the first 55% of the time required to cool the Thingmuli magma its erupted lavas would be

olivine tholeiitic and tholeiitic in composition. During this initial interval, the temperature of the magma would be lowered by about 85°. The next 30% of elapsed cooling time produces a temperature drop of 65° C and residual liquids of basaltic andesite composition. The remaining 15% of the cooling interval spans a temperature of 250° C and encompasses the period of generation of icelanditic and more siliceous residual liquids. If eruptions at the Thingmuli volcanic center were periodic in time and our interpretation of cooling rate from Fig. 10 is correct, then volumetric considerations were clearly not the only factor in determining the compositional diversity of the erupted lavas. Additionally, the fine structure of the cumulative heat curve (the pulses or spikes in the latent heat of crystallization) indicates that the cooling rate was probably not a smooth function of temperature.

Free energy of crystallization

In Fig. 11 the Gibbs free energy differences between the supercooled liquid and the stable liquid + solid assemblage are plotted for each, 1 bar, fractionation interval of the Thingmuli olivine tholeiite. Note, as in the example of equilibrium crystallization of the Jorullo basaltic andesite, that these energy differences are small. The degree of supersaturation and the associated energy released during precipitation are provided in Table 7. One interesting aspect of this open system calculation is that at advanced stages of fractionation, the supercooled liquid has a lower free energy than the calculated stable liquid + solid assemblage. This point in the cooling history occurs in Fig. 11 where the free energy change goes to zero and subsequently becomes negative. It corresponds exactly to the beginning of a net increase in the oxygen content of the system (where ΔO_2 passes through zero in Fig. 6). The thermodynamic stability of the calculated solid + liquid assemblage at temperatures where ΔG (Fig. 11 and Table 7) is negative can be understood if it is realized that the Korzhinskii potential (Thompson 1970), not the Gibbs free energy, of an open system is minimized at equilibrium (Part I). Figure 11 demonstrates that the minimum in these two functions is not necessarily coincident.

A new liquid variation diagram

The ability of silica activity to illuminate the interpretation of common phenocryst parageneses in volcanic rocks (Carmichael et al. 1970; Nicholls et al. 1971) has led Carmichael et al. (1974) to develop the idea that the stable phenocryst assemblages and the essential compositional variability of the majority of igneous rocks can be expressed in terms of the activities of the components silica and soda in the melt. In choosing silica activity to link rock composition to mineral paragenesis, Carmichael et al. (1974) have improved upon Shand's (1943) original concept of silica saturation. In Fig. 12a we have extended Carmichael et al.'s (1974) idea by constructing an activity of soda ($Na_{16/3}Si_{8/3}O_8$ is the liquid component of Ghiorso et al. 1983, which proxies for Na_2O) versus activity of silica diagram which displays important mineral stability fields and the course of fractional crystallization of the Thingmuli olivine tholeiite. Various rock types and experimental results are also indicated in the figure and are described in the legend. The positions of these data have been calculated directly from
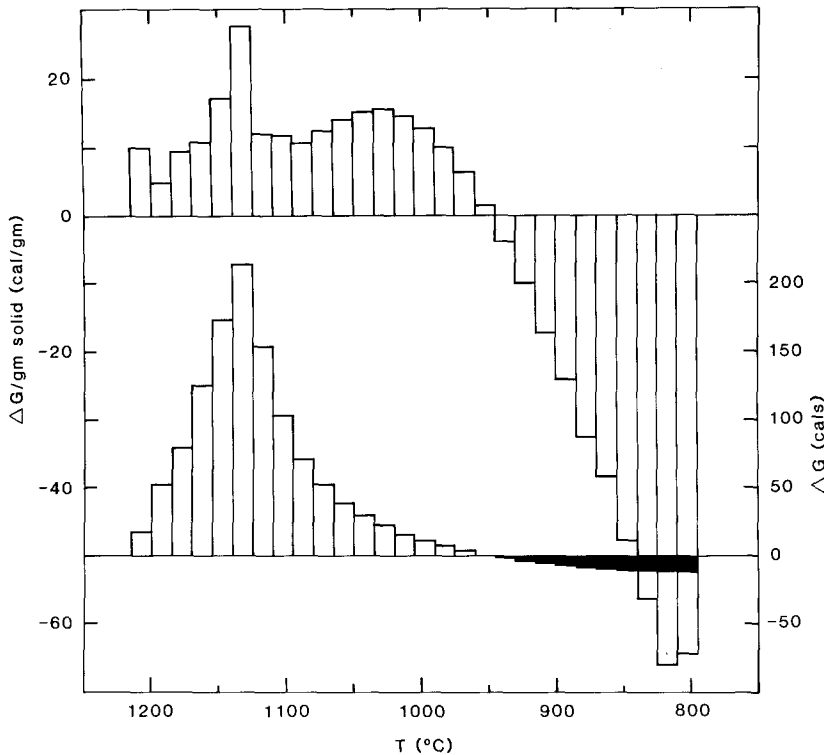
Fig. 11. Bargraphs of the calculated difference in the Gibbs free energy of the multi-phase system and the Gibbs free energy of a metastable liquid of equivalent bulk composition for each cooling interval in the fractional crystallization of an olivine tholeiite (Carmichael 1964a) along the QFM buffer at 1 bar. The cooling interval corresponds to 15° C which is taken as the width of each rectangle. The lower graph describes this energy difference directly in calories and should be read according to the right hand scale. The height of each rectangle in the upper graph has been adjusted for the amount of solid produced in each cooling interval. It should be read according to the left hand scale. The apparently metastable nature of the solid-liquid assemblages at lower temperatures is a consequence of the open system calculations (see text)

Table 7. Thingmuli fractionation: solids crystallized and the degree of supersaturation

T (°C)	ol	opx	plag	cpx	sp	total	ΔG
1,200	1.55		0.17			1.68	17.01
1,185	2.74		7.80			10.54	52.74
1,170	2.22		6.08			8.30	79.12
1,155	1.66		5.84	4.05		11.55	126.70
1,140	1.33		4.66	4.08		10.07	173.60
1,125	1.18		3.61	2.99		7.78	213.90
1,110	0.88		4.85	4.86	2.14	12.73	154.15
1,095	0.52		3.51	3.14	1.53	8.70	103.25
1,080		0.99	2.89	1.80	1.03	6.71	71.57
1,065		0.59	1.92	1.06	0.61	4.18	52.27
1,050		0.35	1.36	0.68	0.39	2.78	39.31
1,035		0.21	1.02	0.46	0.27	1.96	29.86
1,020		0.13	0.80	0.33	0.20	1.46	22.53
1,005		0.08	0.65	0.25	0.15	1.13	16.59
900			0.25	0.05	0.04	0.34	−5.88
810			0.16	0.01	0.02	0.19	−12.57

the liquid composition using the present regular solution model for silicate melts (Ghiorso et al. 1983).

Figure 12a possesses several advantages over typical variation diagrams for displaying the course of crystallization of the Thingmuli olivine tholeiite. To begin with, the activity of soda magnifies the variation in wt % Na_2O seen in Fig. 6. This fact, coupled with the smooth relationship of silica activity to degree of fractionation, allows a straight-forward parameterization of the variation curve shown in Fig. 12a to temperature. This parameterization is, in fact, monotonic; that is, equal decrements in temperature correspond to roughly equal segments of the curve over its *entire* length. This is definitely not a property of the normal

Harker variation diagram (see Fig. 6). Another feature of Fig. 12a is the geometric visualization of the distance between any residual liquid composition and the solid-solid reaction boundaries. Thus, as the liquid approaches the Fo−En boundary we anticipate the impending reaction rather than infer its occurrence from a kink in a curve in Fig. 6.

In addition to reaction relations involving silica any mineral saturation surface can be displayed in Fig. 12a. We could show, for example, a vertical line in activity of soda-silica space corresponding to the saturation surface for olivine of a particular Fo mole fraction coexisting with a liquid of a specified MgO content. The most illuminating mineral phase to so display is plagioclase (Carmichael et al. 1974). Its saturation surface projects from an aluminum activity axis onto the plane in Fig. 12a to form a set of parallel lines, each of which has slope $-10/3$.[5] These lines and their relationship to the Thingmuli trend are indicated in the activity diagram displayed in Fig. 12b. Any specific line corresponds to a specific plagioclase composition or melt aluminum activity. In the case of the Thingmuli series, the plagioclase saturation line which passes through the initial composition corresponds to a projected saturation surface for Ab_{18}, while that which passes through the final composition is Ab_{75}. As the evolution of aluminum activity

---

5 Plagioclase saturation:
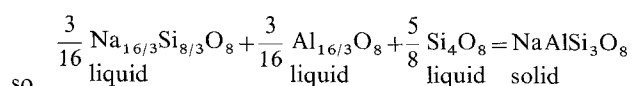
$$\frac{3}{16} \underset{\text{liquid}}{Na_{16/3}Si_{8/3}O_8} + \frac{3}{16} \underset{\text{liquid}}{Al_{16/3}O_8} + \frac{5}{8} \underset{\text{liquid}}{Si_4O_8} = \underset{\text{solid}}{NaAlSi_3O_8}$$

so

$$\log a^{\text{liquid}}_{Na_{16/3}Si_{8/3}O_8}$$

$$= \left(-\frac{16}{3} \log K + \log a^{\text{liquid}}_{Al_{16/3}O_8} + \frac{16}{3} \log a^{\text{plag}}_{NaAlSi_3O_8} \right)$$

$$- \frac{10}{3} \log a^{\text{liquid}}_{Si_4O_8}$$
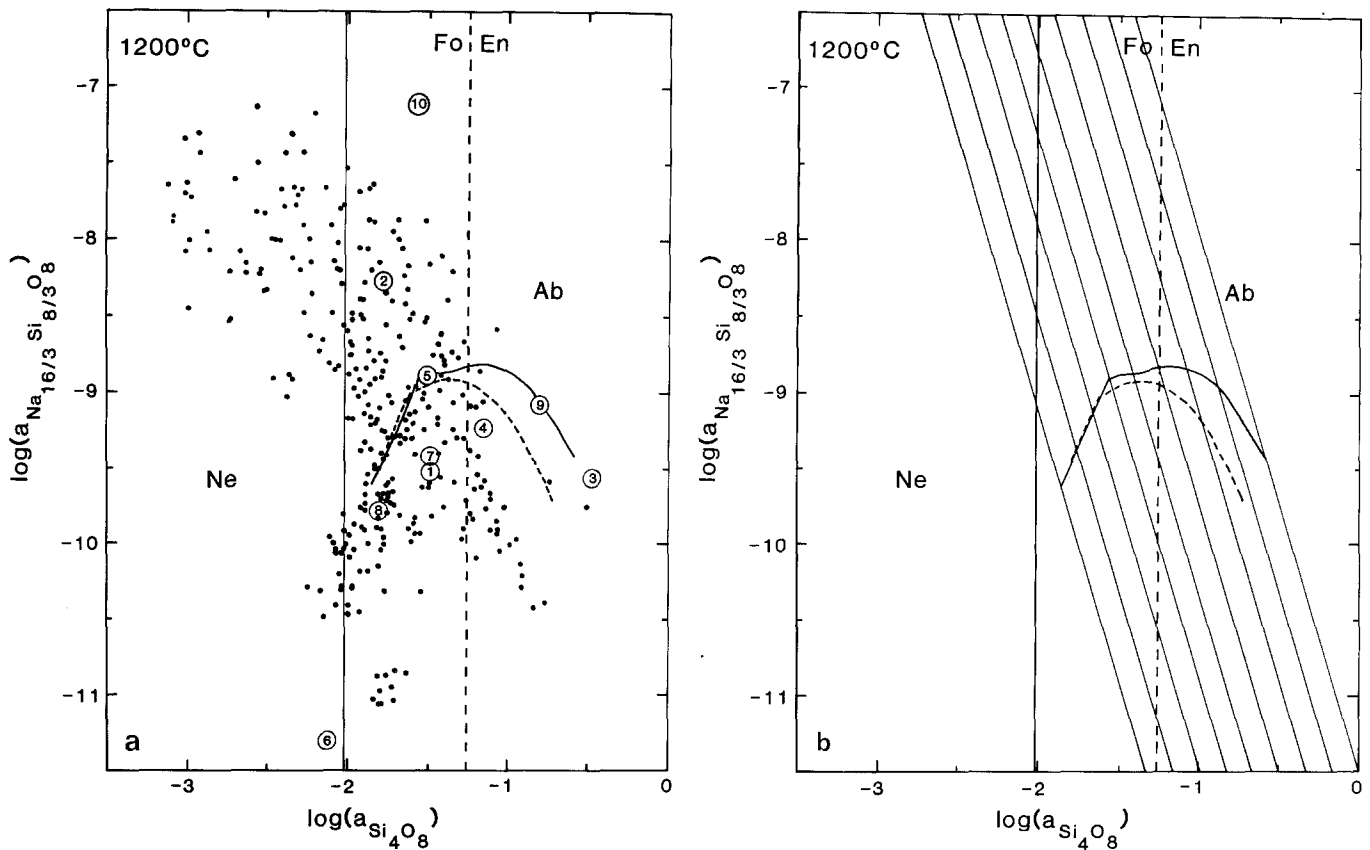
Fig. 12a and b. Activity-activity diagram for the system $Na_2O-Al_2O_3-SiO_2$ at 1,200° C and 1 bar. The vertical dotted line denotes the silica activity corresponding to a unit activity ratio of $a_{Mg_2SiO_4}^{olivine}/a_{Mg_2Si_2O_6}^{orthopyroxene}$. The solid line connects calculated melt activities for each cooling interval in the fractional crystallization of an olivine tholeiite (Carmichael 1964a) along the QFM buffer at 1 bar. The dotted line denotes similar calculations at two kilobars. The crystallization interval was 15° C. All calculated activities have been normalized to a constant temperature (1,200° C). **a** The numbered points denote liquid activities calculated at 1,200° C for lavas of various bulk compositions: 1) Quartz basalt (CAL 20, Smith and Carmichael 1968), 2) Olivine basalt (SSC 2, Brown and Carmichael 1971), 3) Rhyolite (CAM 73, Carmichael 1967b), 4) Andesite (COL 7, Luhr and Carmichael 1980), 5) Tholeiite (Carmichael 1964a), 6 and 8) Komatiite (Nisbet et al. 1977), 7) Tholeiite (Philpotts 1979), 9) Dacite (N. 67, Nelson 1979), 10) Phonolite (3G, Carmichael 1964b). The solid circles represent all the melt compositions used by Ghiorso et al. (1983) to calibrate the liquid solution model upon which all the mass transfer calculations in this paper are based. **b** The solid lines with slope $-10/3$ denote the trace of the plagioclase saturation surface. The line farthest right corresponds to Ab_{75} while that farthest left corresponds to Ab_{18}. Note the angle of intersection of the Thingmuli fractionation path with the plagioclase saturation surface at intermediate compositions. The significance of this angle is discussed in the text

in the Thingmuli lavas is essentially linear, a family of lines corresponding to intermediate plagioclase contents can be drawn between these two extremes. Thus, liquids following the Thingmuli fractionation curve successively cut plagioclase saturation surfaces of increasing albite content. The more the slope of the fractionation curve in Fig. 12b approaches 3/10, the more rapid the shift in plagioclase composition with crystal fractionation. Hence, plagioclase composition changes most rapidly with increasing silica activity in the basaltic andesites, less so in the olivine tholeiites and tholeiites, and least rapidly in the icelandites and rhyolites.

Even without detailed knowledge of the variation in liquid activities, the geometry of any fractionation curves displayed in Fig. 12 in relation to the topology of the activity/saturation diagram provides more critical insight into the relationship between melt and phenocryst composition than can be obtained from any more traditional variation diagram. Given the current ease of calculating activities of melt components (Ghiorso et al. 1983) we advocate the

extensive use of such diagrams in interpreting the crystallization history of igneous rocks.

Comparison of equilibrium and fractional crystallization

It is intriguing to consider the course of crystallization of the Thingmuli tholeiite in equilibrium rather than fractionation mode. Although there are no natural or experimental data with which to compare, the results of such an open system equilibrium calculation are shown in Fig. 13. Though the figure is largely self-explanatory, it is well to note: (1) the greater latent heat of crystallization when compared to Fig. 10, (2) the close correspondence of the lowest temperature assemblage (solidification took place at about 1,040° C) to the CIPW norm, and (3) the liquid density turnover and silica increase initiated by the precipitation of spinel. This equilibrium calculation shows that the reaction relationship between olivine and orthopyroxene takes place over a finite temperature interval.
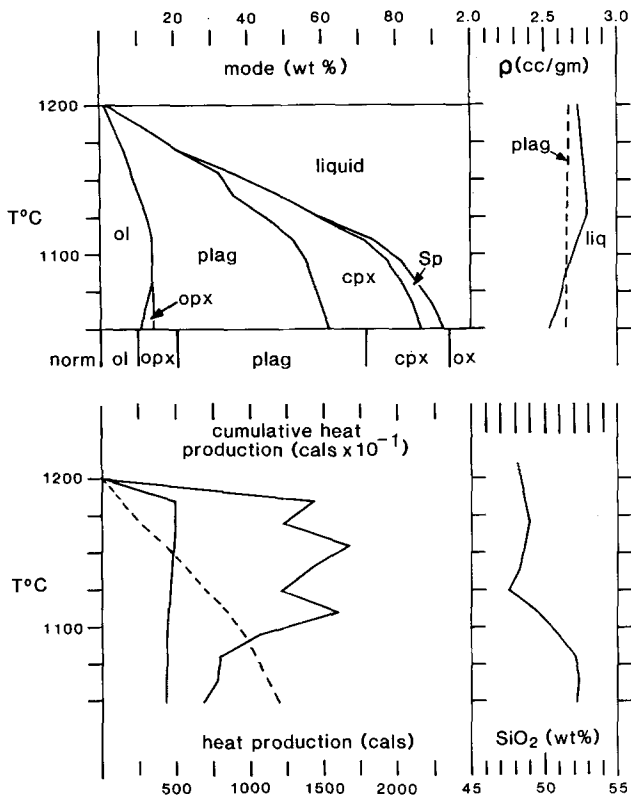
Fig. 13. Results of calculations on the equilibrium crystallization of an olivine tholeiite (Carmichael 1964a) along the QFM buffer at 1 bar. The crystallization interval was taken to be 15° C and the results at each temperature are shown connected by continuous lines. *Upper left*: Note that the liquid solidifies completely between 1,050° C and 1,035° C. The line labeled norm corresponds to the calculated QFM CIPW norm at 1,200° C. *ol*, olivine; *opx*, orthopyroxene; *plag*, plagioclase; *cpx*, clinopyroxene; *ox*, oxides. *Upper right*: Note how the density of plagioclase remains less than the density of the melt until more than 80% of the liquid has crystallized. *Lower left*: This portion of the figure is labeled identically as Fig. 10. *Lower right*: Note that the substantial increase in melt silica content is triggered by the precipitation of spinel

Low pressure crystallization of an olivine boninite

The previous two examples have explored aspects of the equilibrium and fractional crystallization of lavas which produce the sequence of phases olivine, plagioclase, augite then spinel and/or pigeonite successively on the liquidus. As a final example we turn to a magma composition whose order of crystallization reflects more closely that observed in large basic layered intrusions, namely: olivine, orthopyroxene, then plagioclase and/or clinopyroxene. The initial liquid composition for this example is taken from Irvine and Sharpe (1982) and represents the intrusive equivalent of a slightly olivine-enriched boninite (liquid U 1, CO255, or their Table 10). This liquid composition, hereafter referred to as U 1, is based on analyses of chilled margins of sill offshoots of the Bushveld complex reported in Sharpe (1981). The importance of understanding the crystallization behavior of magmatic liquids like U 1 in interpreting mineral parageneses in the Stillwater and the Bushveld complex has been discussed by Irvine (1983).

Results of the calculation are shown in Figs. 14–17. The calculation was performed using 25° C temperature incre-

ments, in open system mode (see above) along the QFM buffer, to facilitate comparison with experimental data on similar liquids reported by Cawthorn and Davies (1983) and Sharpe and Irving (1983). Due to the late appearance of spinel (Fe—Ti oxide) the results of closed system calculations closely resemble those reported here.

With the exception of the absence of chromite, which was suppressed as a product phase, the calculated mineral sequence shown in Fig. 14 closely resembles that produced by the Bushveld magma (Wager and Brown 1967). The similarity extends to the prolonged interval of olivine/orthopyroxene precipitation, the rapid appearance of clinopyroxene following that of plagioclase, the lengthy period of cotectic precipitation of orthopyroxene-plagioclase-clinopyroxene, and the late appearance of Fe—Ti oxides. Calculated mineral compositions are compared to their Bushveld counterparts at each stage in the sequence in Table 8.

Experimental data are available on the *equilibrium* crystallization of liquids similar in composition to U 1. Sharpe and Irvine (1983) report one atmosphere melting experiments, performed along the QFM buffer, on a U 1 type rock whose composition is reported in Sharpe et al. (1983). These experimental results are shown in Fig. 14. Sharpe and Irvine's composition, labeled U 1b, contains almost 5 wt % MgO less than U 1 and undoubtedly this is reflected in its lower liquidus temperature and contracted interval of olivine precipitation. The experimental liquidus temperature for clinopyroxene can be extrapolated from Sharpe and Irvine's results to be about 1,110° C. This is in good agreement with the calculations displayed in Fig. 14. Unfortunately, these authors provide no compositional data on the phases. Cawthorn and Davies (1983) report crystallization experiments, at low (?) f_{O_2} and 3 kbars pressure, on a liquid composition (#4, Buffelsfontein sill, 344JQ) which contains about 2 wt % less MgO than U 1. This liquid, like Sharpe and Irvine's (1983) U 1b, corresponds to a sample obtained from one of the marginal sills of the Bushveld intrusion. Like U 1, it has been postulated to represent the composition of a Bushveld parental magma. Cawthorn and Davies (1983) report the sequence olivine (1,300° C), olivine out/orthopyroxene in (1,250° C), plagioclase (1,166° C), clinopyroxene (1,150° C), chromite (1,120° C). Given the importance of oxygen fugacity in controlling the appearance temperatures of mafic phases in these liquids (Sharpe and Irvine 1983), it is difficult to compare Cawthorn and Davies' experiments to the results of Fig. 14 except to say that they are broadly similar and that their study indicates a much expanded field of olivine crystallization at low pressure (1 bar). They do report an orthopyroxene composition (En_{82} at 1,166° C) corresponding to the first appearance of plagioclase, which is about 7 mole % higher than that calculated here or *observed* in the Bushveld rocks (Table 8).

One of the extraordinary features of the calculation displayed in Fig. 14 is the extended interval of crystallization. Some 400° C after the first appearance of olivine the liquid is not quite 80% crystallized. This provides a marked contrast when compared to the crystallization of the olivine tholeiite described above. To extend the comparison further, it should be noted that in the crystallization of this magma there is no interval of plagioclase floatation (Fig. 14) and the heat production associated with crystallization far exceeds that of the tholeiite. The substantial heat output associated with reaching the plagioclase, orthopyroxene, clinopyroxene cotectic would presumably have a
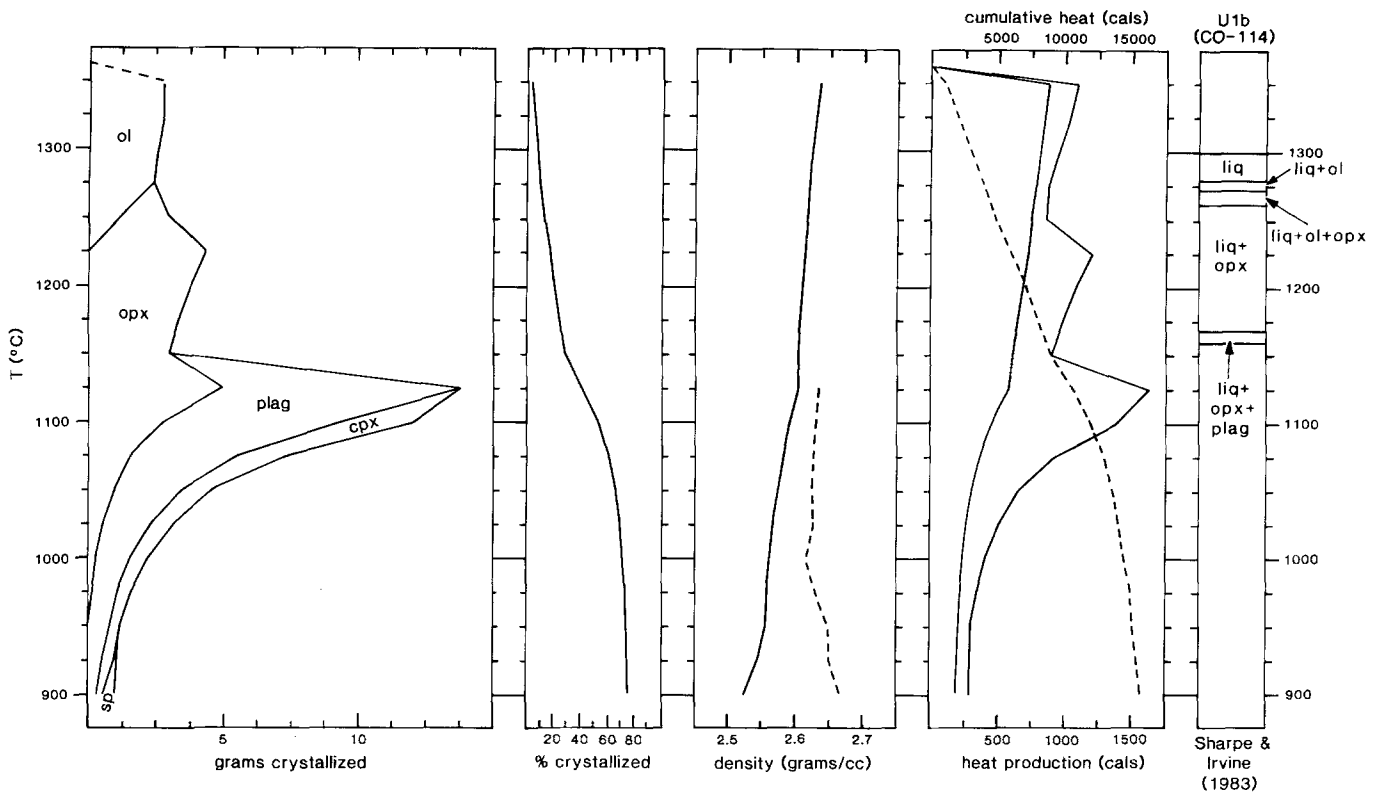
Fig. 14. Results of calculations on the fractional crystallization of an olivine boninite (U 1, Irvine and Sharpe 1982) along the QFM buffer at 1 bar. The crystallization interval was taken to be 25° C and the results at each temperature are shown connected by continuous lines. *Far left*: Mass of material solidified during each interval of the crystallization history. Initial liquid mass was 100 g. *Middle left*: Note that after 450° C of crystallization less than 80% of the melt has solidified. *Middle*: Solid line is the density of the liquid and the dotted line is the density of the coexisting plagioclase. Note that the plagioclase is always more dense than the melt. *Middle right*: This portion of the figure is labeled identically as Fig. 10. *Far right*: Experimental 1 bar crystallization data on a less MgO-rich olivine boninite. Experiments were conducted between 1,300° and 1,160° C along the QFM buffer (Sharpe and Irvine 1983)
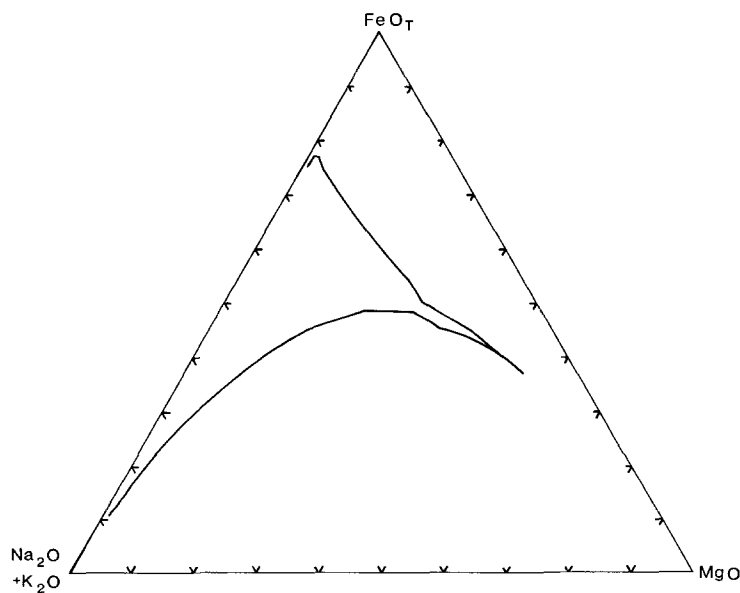
Fig. 15. Calculated liquid paths for the fractional (upper curve) and equilibrium (lower curve) crystallization of an olivine boninite (U 1, Irvine and Sharpe 1982) along the QFM buffer at 1 bar. The crystallization interval was taken to be 25° C and results at each temperature are shown connected by solid lines. FeO_T denotes the total iron content of the melt expressed at FeO. The diagram is in wt %

profound impact on the thermal regime of any magma chamber crystallizing liquids of this composition.

In Fig. 15 liquid compositions are plotted which describe both the equilibrium and fractional crystallization of U 1 along the QFM buffer at 1 bar. The calculated paths should be compared to that suggested for the Bushveld

complex by Wager and Brown (1967). The turnover at high iron contents in the fractionation curve corresponds to the precipitation of Fe–Ti oxides, and the extreme iron enrichment is due to their late appearance. In Fig. 16, residual liquid compositions from the fractionation calculation are shown on a silica variation diagram. Silica shows a steady
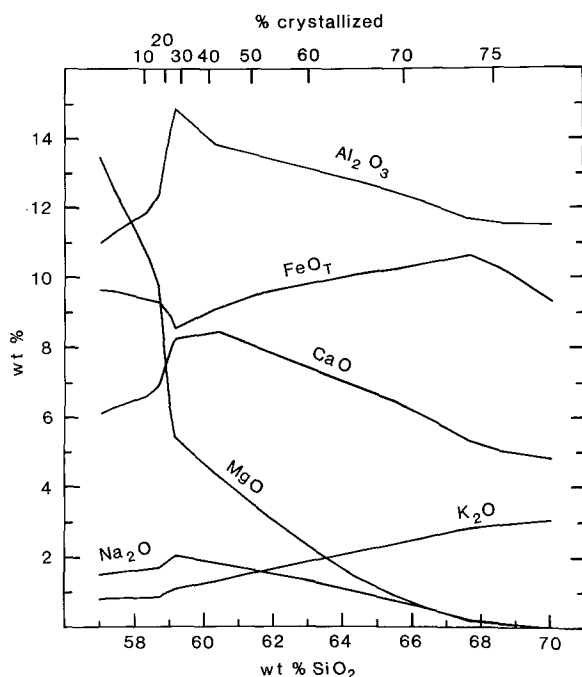
Fig. 16. Calculated liquid variation diagram for the fractional crystallization of an olivine boninte (U 1, Irvine and Sharpe 1982) along the QFM buffer at 1 bar. The crystallization interval was taken to be 25° C and results at each temperature are shown connected by solid lines. Note the wt % crystallization scale which labels the top of the diagram. FeO_T denotes the total iron content of the melt expressed at FeO

Fig. 17. Calculated pyroxene compositions precipitated during the fractional crystallization of an olivine boninite (U 1, Irvine and Sharpe 1982) along the QFM buffer at 1 bar. The crystallization interval was taken to be 25° C and results at selected temperatures are shown. *Coexisting* pyroxene compositions are linked by lines rather than being denoted individually by solid circles. The diagram is in mole %

Table 8. Comparison of mineral compositions

Bushveld paragenesis	Bushveld intrusion (Wager and Brown 1967)	Fractional crystallization of U 1
Upper zone		
olivine	$Fo_{49} - Fo_0$	not present
plagioclase	$An_{53} - An_{30}$	An_{52}
orthopyroxene	$En_{41} - En_{31}$	En_{41}
clinopyroxene	$Ca_{38}Mg_{33}Fe_{29}$ $- Ca_{42}Mg_1Fe_{57}$	$Ca_{44}Mg_{22}Fe_{34}$ $- Ca_{44}Mg_{20}Fe_{36}$
magnetite	–	$Uv_{60} - Uv_{58}$
Main zone + upper critical series		
plagioclase	$An_{77} - An_{53}$	$An_{53} - An_{49}$
orthopyroxene	$En_{75} - En_{44}$	$En_{70} - En_{48}$
clinopyroxene	$Ca_{44}Mg_{46}Fe_{10}$ $- Ca_{38}Mg_{33}Fe_{29}$	$Ca_{42}Mg_{38}Fe_{19}$ $- Ca_{43}Mg_{24}Fe_{32}$
Lower critical series		
plagioclase	An_{78}	An_{57}
orthopyroxene	En_{75}	En_{74}
Basal series		
olivine	$Fo_{88} - Fo_{86}$	$Fo_{89} - Fo_{84}$
orthopyroxene	En_{83}	$En_{84} - En_{78}$

of U 1 are plotted in fig. 17. These should be compared to the Bushveld data reported in Table 8. The trend in clinopyroxene compositions deviates from that expected at more advanced stages of fractionation, as in the olivine tholeiite calculation. The unexpectedly high Na-content of the initial plagioclase crystals may in part cause this trend, in that postponed removal of CaO from the liquid produces a relative enrichment at the latter stages of crystallization and a correspondingly high-Ca clinopyroxene.

The calculations presented in this example form a test as to the ability of the thermodynamic model (Ghiorso et al. 1983) to predict phase relations in liquids substantially unlike those upon which it was calibrated. The results are encouraging, though not as conclusive as those of the basaltic andesite or olivine tholeiite. However, any failings clearly show the need to determine plagioclase-melt relations in such liquids and demonstrate the lack of phase-equilibrium data relating the compositions of clinopyroxene, orthopyroxene, olivine and liquid in the more siliceous residual melts.

increase with degree of crystallization. The initial sharp decrease in MgO and increase in Al_2O_3 and CaO are related to the interval of olivine and orthopyroxene precipitation, while the subsequent reversal in the Al_2O_3, CaO and FeO_T trends reflects the formation of plagioclase. The ultimate decrease in FeO_T is a response to the precipitation of spinel. An examination of the calculated mineral compositions reported in Table 8 reveals that the formation of a relatively sodic plagioclase causes the crossover in the alkali variation curves in Fig. 16. As the calculated plagioclase compositions are at variance with those found in the intrusion, the soda variation curve of Fig. 16 may be inappropriate.

The calculated compositions of orthopyroxene and clinopyroxene produced during the fractional crystallization

Examples of assimilation calculations

Assimilation of olivine into a quartz dioritic liquid

In his classic paper on the assimilation of solid inclusions, Bowen (1922) outlined the general effects produced during the reaction of basic igneous rocks with more silica-rich magmatic liquids. As a quantitative illustration of his premise that acid magmas *react* with rather than dissolve incorporated basic inclusions, Bowen considered the assimilation of forsterite into a binary liquid saturated with clino-enstatite in the system $Mg_2SiO_4 - SiO_2$. The conclusions he draws from an analysis of this simple example offer profound insight into an important process in magma genesis.

138

Bowen (192, p. 533–536) writes of the assimilation of forsterite that:

"... it should be noted that the amount of clino-enstatite formed is not simply the chemical equivalent of the forsterite changed... [but is] ...in fact above five times [by weight] the amount of forsterite... for the liquid cannot have excess silica subtracted from it without passing under the clino-enstatite saturation curve." "...the reaction is in fact, exothermic...[and]...results in a diminution in the amount of liquid and a corresponding increase in the amount of solids even when this heating effect takes place. If heat is being taken from the system this process would act as a deterrent upon the rate of cooling."

Bowen concludes that in the assimilation of any basic inclusions which contain minerals that bear a reaction relationship to solid phases presently in equilibrium with the reacting liquid, the effects observed in the simple system example will be manifest, namely: (1) the process will generate heat, and (2) more solid will be produced than consumed *even* if all the liberated heat is utilized in raising the temperature of the melt. Though not specifically stated by Bowen, it follows from his second generalization, and the fact that most igneous minerals have negative volumes of crystallization, that the net effect of assimilating a basic inclusion into an acid melt will be to decrease the total volume of the system. To illustrate how the calculational techniques of Part I bear on the problem of solid phase assimilation in magmas, we have chosen to model the process which Bowen envisioned, but was forced to consider in terms of simpler systems, namely the assimilation of olivine into a magma of quartz dioritic composition.

The initial system composition for this example is taken from Erikson (1977) and represents a typical quartz diorite. Iron, expressed as $Fe_2O_{3(T)}$ in the original analysis, is distributed between its two oxidation states by setting the initial system oxygen fugacity according to the QFM buffer. For the purposes of this calculation the magma is considered to be dry and at a fixed temperature and pressure of 1,125° C and 3 kbars, respectively. During the course of assimilation the magma is closed to oxygen exchange with its surroundings and the precipitated solids are allowed to re-equilibrate with the coexisting liquid.

Initial phase relations prior to olivine assimilation are reported in Table 9. With roughly 45% crystallization of orthopyroxene and plagioclase, the composition of the initial liquid is indicated graphically on the left-hand side of

fig. 18. The results of the isothermal, equilibrium, assimilation of olivine (Fo_{90}) into this solid/liquid assemblage are tabulated in Table 9 and displayed in Fig. 18. An examination of Table 9 reveals that all of Bowen's conjectures about the outcome of this rather complex process were correct. The assimilation of olivine generates heat and produces a net increase in solid material. There is, in turn, a net volume decrease for each gram of solid added. Theoretically, these effects should continue until the remaining liquid saturates with the assimilating phase. The calculation reported in Table 9 shows that 20 g of olivine reacting with 100 g of initial material does not bring the system appreciably closer to this theoretical limit.

As the system assimilates more and more olivine the MgO content of the liquid remains essentially constant (Fig. 18) while the liquid FeO content decreases markedly. This is due to the formation of larger and larger amounts of successively more magnesian orthopyroxene, and ultimately, clinopyroxene. Perhaps the most remarkable result of this calculation is the interdependence of the compositions and proportions of all the phases in the system on the assimilation process. For example, as the orthopyroxene increases in abundance and becomes more enstatitic, excess plagioclase precipitates maintaining the Na_2O and CaO contents of the liquid. These results reveal that the reaction stoichiometry is a complex function of the amount of assimilated olivine.

The oxygen fugacity of the liquid steadily increases as a result of the assimilation process. This is due to the steady decrease in FeO and increase in Fe_2O_3 contents in the liquid which accompany the precipitation of orthopyroxene and concentration of residual components (Fig. 18). Oxygen fugacities attained after 20 g of olivine assimilation approach those of the magnetite-hematite buffer. Clearly, isothermal assimilation of olivine into quartz dioritic magma effectively oxidizes the liquid unless oxygen metasomatism or internal homogeneous redox equilibria play an active role in maintaining a buffered state in the magma.

The heat production values indicated in Table 9 correspond to a temperature rise of 3 to 4° C per gram of assimilated olivine. This value is somewhat high, however, because less solid precipitates from the liquid as the temperature of the system increases. Exploratory calculations reveal that a rise of 2° C per gram of assimilated olivine maintains the system in an approximately adiabatic condition throughout the process. We report the results of this "adia-

Table 9. Results of assimilation calculation at constant temperature: 1,125° C (closed system). Initial system mass: 100 g

Grams of Fo_{90} at 1,125° C	opx (grams)	cpx (grams)	plag (grams)	ΔH (cals)	ΔV (cm^3)	Δ grams (solids)
	10.32 (En_{73})		34.50 (An_{31})			
1.0	12.13 (En_{73})		35.35 (An_{32})	− 122.28	− 0.079779	1.66
2.0	13.90 (En_{74})		36.18 (An_{32})	− 118.15	− 0.078174	1.60
3.0	15.64 (En_{75})		36.98 (An_{32})	− 114.46	− 0.076746	1.54
4.0	17.34 (En_{75})		37.77 (An_{32})	− 111.19	− 0.075480	1.49
5.0	19.02 (En_{76})		38.55 (An_{32})	− 108.30	− 0.074359	1.46
6.0	20.65 (En_{76})	0.06 ($_{42}\Delta^{42}$)[a]	39.31 (An_{33})	− 108.64	− 0.075448	1.45
7.0	22.20 (En_{77})	0.27 ($_{42}\Delta^{42}$)	40.08 (An_{33})	− 114.15	− 0.080179	1.53
8.0	23.74 (En_{77})	0.47 ($_{43}\Delta^{42}$)	40.83 (An_{33})	− 111.91	− 0.079265	1.49
9.0	25.25 (En_{78})	0.67 ($_{43}\Delta^{42}$)	41.58 (An_{33})	− 109.98	− 0.078475	1.46
10.0	26.76 (En_{78})	0.86 ($_{43}\Delta^{42}$)	42.32 (An_{33})	− 108.30	− 0.077791	1.44
20.0	41.34 (En_{82})	2.61 ($_{46}\Delta^{42}$)	49.47 (An_{34})	− 98.75	− 0.073540	1.29

[a] Clinopyroxene composition denoted by $_a\Delta^b$, where a refers to mole % $Mg_2Si_2O_6$ and b refers to mole % $Ca_2Si_2O_6$
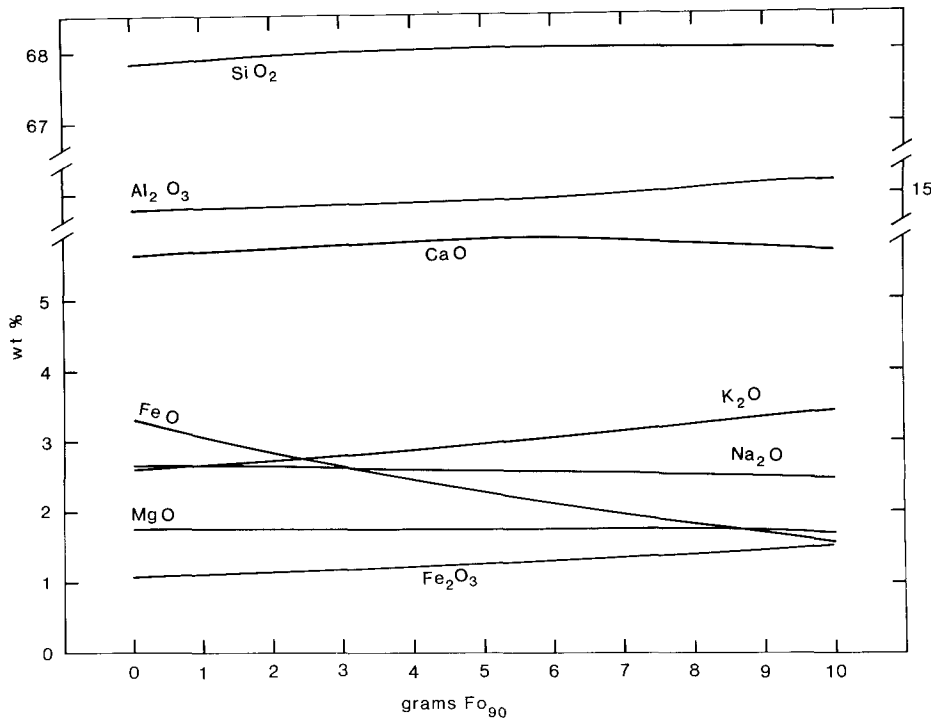
Fig. 18. Calculated liquid variation diagram due to the assimilation of olivine (Fo_{90}) into an equilibrium assemblage of orthopyroxene, plagioclase and liquid, initially of quartz dioritic composition (after Erikson 1977), along the QFM buffer at three kilobars and 1,125°. The initial system has a mass of 100 g. The quantity of assimilated olivine is indicated on the abscissa. Olivine was assimilated in one gram increments and solid lines connect the plotted results. Table 9 should be consulted for the relative proportions of the solids and liquids, the solid compositions and the heat effects produced during this assimilation calculation. Note the two breaks in the ordinate

Table 10. Results of assimilation calculation at "constant" enthalpy and variable T (Closed system). Initial system mass: 100 g

T (°C)	grams of Fo_{90} at 1,125° C	opx (grams)	plag (grams)	ΔH (cals)	ΔV (cm³)	Δ grams (solids)	ΔH^a	$\rightarrow T^b$ °C
1,125		10.22 (En_{73})	32.21 (An_{33})					
1,127	1.0	11.87 (En_{74})	32.43 (An_{33})	−18.20	−0.054515	0.87	−12.72	0.41
1,129	2.0	13.47 (En_{74})	32.63 (An_{33})	−14.16	−0.053435	0.80	− 9.29	0.30
1,131	3.0	15.05 (En_{75})	32.83 (An_{34})	−10.48	−0.052485	0.787	− 6.22	0.20
1,133	4.0	16.61 (En_{76})	33.02 (An_{34})	− 7.12	−0.051645	0.75	− 3.47	0.11
1,135	5.0	18.15 (En_{76})	33.20 (An_{34})	− 4.02	−0.050896	0.72	− 0.98	0.03
1,137	6.0	19.66 (En_{77})	33.38 (An_{34})	− 1.15	−0.050222	0.69	1.28	−0.04
1,139	7.0	21.16 (En_{77})	33.55 (An_{35})	1.55	−0.049606	0.67	3.38	−0.10
1,141	8.0	22.65 (En_{78})	33.71 (An_{35})	4.11	−0.049035	0.65	5.33	−0.16
1,143	9.0	24.12 (En_{78})	33.86 (An_{35})	6.56	−0.048496	0.62	7.17	−0.22
1,145	10.0	25.59 (En_{79})	34.01 (An_{36})	8.94	−0.047976	0.62	8.94	−0.27
Total:				−33.97	−0.508311[c]	7.17	− 6.58	0.26

[a] Includes heat necessary to take remaining grams of olivine up in temperature (olivine $Cp \simeq 0.3043$ cal/K-grm)

[b] ΔH converted to temperature using the system Cp

[c] System volume is about 39.303120 cm³. This is a decrease of 1.29%

batic" assimilation of olivine in Table 10 and Fig. 19 to illustrate Bowen's (1922) contention that even under these conditions the mass of solid material formed exceeds that assimilated. As in the example of isothermal assimilation the quantity of orthopyroxene *and* plagioclase increase as olivine reacts with the liquid. As assimilation proceeds their compositions become more enstatitic and more anorthitic, respectively. It should be noted that the rise in temperature prevents the intersection of the clinopyroxene liquidus.

The liquid variation diagram for this adiabatic assimilation (Fig. 19) shows some marked differences when compared to that of the isothermal calculation (Fig. 18). The silica weight fraction decreases with reaction progress in Fig. 19 as does FeO, but the latter is not so markedly removed from the liquid as to cause the extreme oxidation seen in the isothermal case. The oxygen fugacity of the

final assemblage at 1,145° C is only 3 log units above QFM. The diminished formation of orthopyroxene and plagioclase permit the enrichment of the derived liquids in MgO and Na_2O. One of the more interesting comparisons to be made between Figs. 18 and 19 concerns the behavior of the alkalies, which reflect the very different responses of plagioclase precipitation to the two paths of assimilation studied.

The great advantage of performing assimilation calculations using the procedures outlined in Part I (and utilized in the present examples) is the ability to follow the compositional changes which the phases in the system undergo as the reaction proceeds along a *particular irreversible path* (in this case isothermal or isenthalpic). This generates directly information concerning reaction stoichiometry along this path. By comparing such results with field and petro-
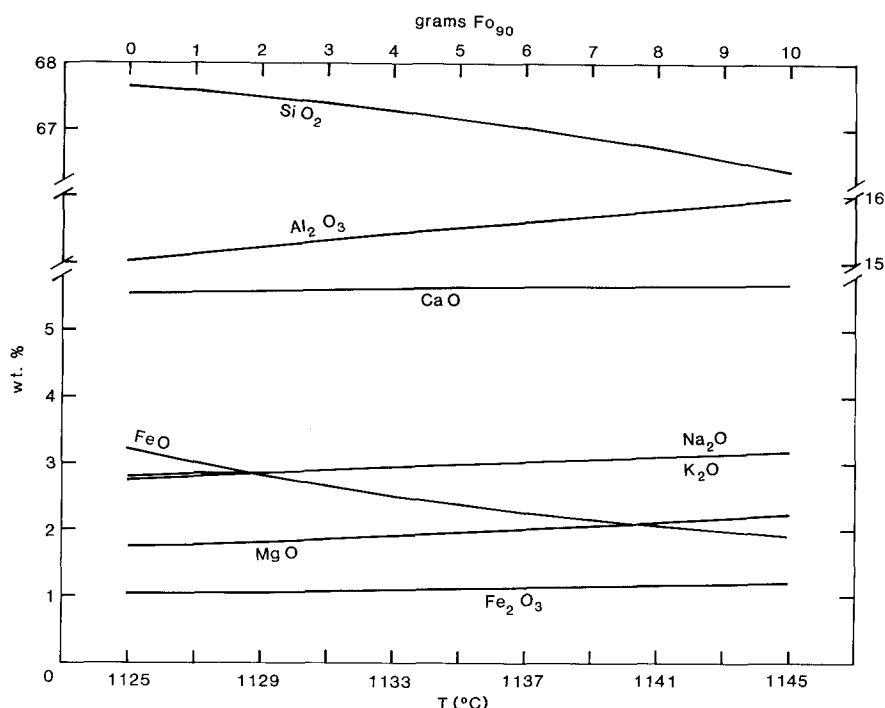
Fig. 19. Calculated liquid variation diagram due to the assimilation of olivine (Fo_{90}) into an equilibrium assemblage of orthopyroxene, plagioclase and liquid, initially of quartz dioritic composition (after Erikson 1977), along the QFM buffer at three kilobars. The initial system has a mass of 100 g. Olivine was assimilated one gram at a time at the rate of 1 g per 2° C increase in temperature. This approximated adiabatic assimilation. Table 10 should be consulted for the relative proportions of the solids and liquids and the solid compositions produced during this assimilation calculation. The Na_2O and K_2O curves substantially overlap. At lower temperatures near 1,125° C the lower of the two curves corresponds to K_2O. Note the two breaks in the ordinate and the two alternative means of labeling the abscissa

graphic observations on arrested assimilation events in igneous rocks, the mechanism of solid phase assimilation can potentially be deduced. A particular reaction stoichiometry might denote the extent of assimilation or whether the process took place under isothermal, isobaric, isenthalpic, or isochoric (etc.) conditions. Nicholls and Stout (1982), in their paper on heat effects of asimilation recognized the importance of understanding the reaction stoichiometry in order to discern the details of the process. It is apparent that only detailed calculations of chemical mass transfer, like those reported here, can hope to substantiate and quantify assimilation mechanisms proposed for magmatic systems.

Conclusions

The examples and calculations reported in this paper demonstrate the advantage of applying a thermodynamic approach to modelling processes describing chemical mass transfer in magmatic systems. The ability to monitor a wide variety of thermodynamic state variables in a complex multicomponent magmatic system, as a function of reaction progress, coupled with the knowledge that the calculated intermediate phase assemblages are in chemical equilibrium, greatly facilitates the evaluation of hypotheses regarding the genesis of igneous rocks.

With these examples we have demonstrated a number of petrological effects which would have been difficult if not impossible to address by more conventional methods of analysis. In particular we have explored the important control oxygen fugacity plays in governing the crystallization paths of basic magmas and commented upon the role of oxygen metasomatism (or hydrogen loss) as an important magmatic process. Our calculations have revealed the details of the heat output of magmatic systems undergoing equilibrium crystallization, crystal fractionation or solid phase assimilation, and have emphasized the small amounts of energy available to drive crystallization process in super-

saturated silicate melts. The importance of these effects to the kinetics of crystallization cannot be over emphasized.

The calculations presented here also indicate the need for further experimental work and refinement of the thermodynamic model. Perhaps the most frustrating difficulty encountered in performing these calculations is the lack of a good solid solution model for the pyroxenes. Restricting attention to pyroxene compositions within the quadrilateral effectively prevents modelling phase relations in alkalic rocks and in basalts at elevated pressures. In addition, lack of experimental information on solid-liquid phase relations in water undersaturated melts and activity/composition relations in amphiboles and micas effectively prevents modelling the chemical evolution of calc-alkaline magmas and siliceous continental lavas.

Despite these limitations we believe the examples of chemical mass transfer provided in this paper substantiate the computational approach outlined in Part I and reaffirm the ability of the silicate liquid solution model of Ghiorso et al. (1983) to accurately predict, insofar as the available experimental data make its calibration possible, the free energies of mixing of natural silicate liquids. In this regard, it is worth re-emphasizing that these free energies of mixing must be known to within 5 or 10 *calories* per gram-formula-weight of liquid in order to correctly calculate the appearance temperatures ($+/-5°$ C), compositions ($+/-2-3$ mole %) and proportions of phases on the liquidus. It is worth bearing this observation in mind when considering the results presented here in terms of the uncertainties in contributing thermodynamic data and the incomplete solid solution models utilized for many of the solid phases.

then the examples presented here. In particular we wish to thank Prof. J. Nicholls, M. Z. Stout, Prof. J.K. Russell, L.J. Criscenti and particularly P.B. Kelemen. Helpful reviews were provided by L.M. Barron, Prof. G. Brimhall, L.J. Criscenti, P. Kelemen, Prof. J. Nicholls, Prof. M. Reed and particularly Prof. J.K. Russell. One of us (ISEC) wishes to acknowledge material support for this investigation from NSF (EAR-81-03344) and the Office of Energy Research, Office of Basic Energy Sciences, Division of Engineering, Mathematics and Geosciences, of the US Department of Energy under contract W-7405-ENG-48. The calculations presented here were performed at the University of Washington where computer time was graciously provided by the College of Arts and Sciences. In this regard the assistance of Prof. J. Adams is greatly appreciated.

References

Aagaard P, Helgeson HC (1982) Thermodynamic and kinetic constraints on reaction rates among minerals and aqueous solutions. I. Theoretical considerations. Am J Sci 282:237–285

Arculus RJ, DeLano JW (1981) Intrinsic oxygen fugacity measurements: techniques and results for spinels from upper mantle peridotites and megacryst assemblages. Geochim Cosmochim Acta 45:899–913 (1981)

Bowen NL (1922) The behavior of inclusions in igneous magmas. J Geol 30:513–570

Brown FH, Carmichael ISE (1971) Quaternary volcanoes of the Lake Rudolf region: II. The lavas of North Island, South Island and the Barrier. Lithos 4:305–323

Buddington AF, Lindsley DH (1964) Iron-titanium oxide minerals and synthetic equivalents. J Petrol 5:310–357

Carmichael ISE (1964a) The Petrology of Thingmuli, a Tertiary volcano in Eastern Iceland. J Petrol 5:435–460

Carmichael ISE (1964b) Natural liquids and the phonolitic minimum. Geolog J 4[pt. 1]:55–60

Carmichael ISE (1967a) The mineralogy of Thingmuli, a Tertiary volcano in Eastern Iceland. Am Mineral 52:1815–1841

Carmichael ISE (1967b) The iron-titanium oxides of salic volcanic rocks and their associated ferro-magnesian silicates. Contrib Mineral Petrol 14:36–64

Charmichael ISE, Ghiorso MS (1985) Oxidation-reduction relations in basic magma: a case for homogeneous equilibria. EPSL (submitted)

Carmichael ISE, Nicholls J, Smith AL (1970) Silica activity in igneous rocks. Am Mineral 55:246–263

Carmichael ISE, Turner FJ, Verhoogen J (1974) Igneous Petrology. McGraw-Hill Book Company, New York, p 739

Cawthorn RG, Davies G (1983) Experimental data at 3 kbars pressure on parental magma to the Bushveld complex. Contrib Mineral Petrol 83:128–135

Dowty E (1980) Crystal growth and nucleation theory and the numerical simulation of igneous crystallization. In: Hargraves, RB (ed) Physics of Magmatic Processes, Princeton Univ Press, Princeton, New Jersey, 419–485

Erikson EH (1977) Petrology and petrogenesis of the Mount Stuart batholith – plutonic equivalent of a high-alumina basalt association? Contrib Mineral Petrol 60:183–207

Ghiorso MS (1984) Activity/composition relations in the ternary feldspars. Contrib Mineral Petrol 87:282–296

Ghiorso MS (1985) Chemical mass transfer in magmatic processes. I. Thermodynamic relations and numerical algorithms. Contrib Mineral Petrol (in press)

Ghiorso MS, Carmichael ISE, Rivers ML, Sack RO (1983) The Gibbs free energy of mixing of natural silicate liquids; an expanded regular solution approximation for the calculation of magmatic intensive variables. Contrib Mineral Petrol 84:107–145

Grove TL, Baker MB (1984) Phase equilibrium controls on the tholeiitic versus calc-alkaline differentiation trends. J Geophys Res 89[B5]:3253–3274

Irvine TN (1983) The J-M Platinum-palladium reef of the Stillwater complex, Montana: II. Origin by double-diffusive convective magma mixing and implications for the Bushveld complex. Econ Geol 78:1287–1334

Irvine TN, Sharpe MR (1982) Source-rock compositions and depths of origin of Bushveld and Stillwater magmas. Carn Instit Wash Yb 81:294–302

Kilinc A, Carmichael ISE, Rivers ML, Sack RO (1983) The ferric-ferrous ratio of natural silicate liquids equilibrated in air. Contrib Mineral Petrol 83:136–140

Korzhinskii DS (1959) Physiochemical basis of the analysis of the paragenesis of minerals. Consultants Bureau, New York, p 142

Luhr JF, Carmichael ISE (1980) The Colima volcanic complex, Mexico. I. Post caldera andesites from Volcan Colima. Contrib Mineral Petrol 71:343–372

Mo X, Carmichael ISE (1985) Liquid-solid equilibria at 1 bar in lavas from Jorullo, Mexico. Contrib Mineral Petrol (submitted)

Mo X, Carmichael ISE, Rivers M, Stebbins J (1982) The partial molar volume of Fe_2O_3 in multicomponent silicate liquids and the pressure dependence of the oxygen fugacity in magmas. Mineral Mag 45:237–245

Myers J, Eugster HP (1983) The system $Fe-Si-O$: Oxygen buffer calibrations to 1,500 K. Contrib Mineral Petrol 82:75–90

Nelson SA (1979) The geology and petrology of Volcan Ceboruco, Nayarit, Mexico. Unpublished PhD Thesis, Univ California (Berkeley), p 79

Nicholls J, Stout MZ (1982) Heat effects of assimilation, crystallization, and vesiculation in magmas. Contrib Mineral Petrol 84:328–339

Nicholls J, Carmichael ISE, Stormer JC Jr (1971) Silica activity and P_{total} in igneous rocks. Contrib Mineral Petrol 33:1–20

Nisbet EG, Bickle MJ, Martin A (1977) The mafic and ultramafic lavas of the Belingwe greenstone belt, Rhodesia. J Petrol 18:521–566

Osborn EF (1959) Role of oxygen pressure in the crystallization and differentiation of basaltic magma. Am J Sci 257:609–647

Osborn EF (1962) Reaction series for sub-alkaline igneous rocks based on different oxygen pressure conditions. Am Mineral 47:211–226

Philpotts AR (1979) Silicate liquid immiscibility in tholeiitic basalts. J Petrol 20:99–118

Sack RO, Carmichael ISE, Rivers M, Ghiorso MS (1980) Ferric-ferrous equilibria in natural silicate liquids at 1 bar. Contrib Mineral Petrol 75:369–376

Sato M (1978) Oxygen fugacity of basaltic magmas and the role of gas-forming elements. Geophys Res Lett 5:447–449

Shand SJ (1943) Eruptive rocks, their genesis, composition, classification, with a chapter on meteorites. Thomas Murby and Co, London, p 460

Sharpe MR (1981) The chronology of magma influxes to the Eastern compartment of the Bushveld complex as exemplified by its marginal border groups. J Geol Soc London 138:307–326

Sharpe MR, Irvine TN (1983) Melting relations of two Bushveld chilled margin rocks and implications for the origin of chromite. Carn Instit Wash YB 82:295–300

Sharpe MR, Irvine TN, Mysen BO, Hazen RM (1983) Density and viscosity characteristics of melts of Bushveld chilled margin rocks. Carn Instit Wash Yb 82:300–305

Smith AL, Carmichael ISE (1968) Quaternary lavas from the southern Cascades, Western U.S.A. Contrib Mineral Petrol 19:212–238

Thompson JB Jr (1970) Geochemical reaction and open systems. Geochim Cosmochim Acta 34:529–551

Wager LR, Brown GM (1967) Layered Igneous Rocks. W H Freeman and Co, San Francisco, p 588

Yoder HS, Tilley CE (1962) Origin of basalt magmas: An experimental study of natural and synthetic rock systems. J Petrol 3:342–352